


2011

Log-Periodic Microstrip Patch Antenna Miniaturization Using Artificial Magnetic Conductor Surfaces

Ahmad Tariq Almutawa

University of South Florida, ahmed.almutawa@gmail.com

Follow this and additional works at: <https://scholarcommons.usf.edu/etd>

 Part of the [American Studies Commons](#), and the [Electromagnetics and Photonics Commons](#)

Scholar Commons Citation

Almutawa, Ahmad Tariq, "Log-Periodic Microstrip Patch Antenna Miniaturization Using Artificial Magnetic Conductor Surfaces" (2011). *Graduate Theses and Dissertations*.
<https://scholarcommons.usf.edu/etd/2982>

This Thesis is brought to you for free and open access by the Graduate School at Scholar Commons. It has been accepted for inclusion in Graduate Theses and Dissertations by an authorized administrator of Scholar Commons. For more information, please contact scholarcommons@usf.edu.

Log-Periodic Microstrip Patch Antenna Miniaturization Using Artificial Magnetic
Conductor Surfaces

by

Ahmad T. Almutawa

A thesis submitted in partial fulfillment
of the requirements for the degree of
Master of Science in Electrical Engineering
Department of Electrical Engineering
College of Engineering
University of South Florida

Major Professor: Gokhan Mumcu, Ph.D.
Thomas Weller, Ph.D.
Jing Wang, Ph.D.

Date of Approval:
June 14, 2011

Keywords: Broadband Antenna, HIS, EBG, FSS, AMC

Copyright © 2011, Ahmad T. Almutawa

Acknowledgments

I would like to thank Dr. Mumcu for being my thesis advisor. As student of Dr. Mumcu, I gained a technical and practical experience in the field of antenna design. I would also like to thank Dr. Weller and Dr. Wang for being part of my thesis committee and Eng. Patrick Nesbitt, Eng. David Cure and Eng. Olawale Ajayi in helping me with my antenna fabrication.

Also, I would like to take this opportunity to thank The Public Authority for Applied Education and Training in Kuwait for giving me a scholarship to have a master degree in electrical engineering in the field of communication.

Table of Contents

List of Tables	ii
List of Figures	iii
Abstract	vi
1 Introduction.....	1
2 Background and Literature Review	7
2.1 Microstrip Patch Antennas and Design Principles.....	7
2.1.1 Microstrip Line Inset-Feed	10
2.1.2 Coaxial-Probe	10
2.1.3 Aperture-Coupled Feed.....	11
2.1.4 Proximity-Coupled Feed.....	12
2.2 Log-Periodic (LP) Antennas	13
2.3 Artificial Magnetic Conductor (AMC) and Electromagnetic Band Gap (EBG) Structures.....	18
2.3.1 Models for Designing EBG/AMC Unit Cells	19
2.3.1.1 The Lumped Element Model	19
2.3.1.2 Full Wave Numerical Modeling	20
2.3.2 EBG/AMC Structures in Antenna Applications.....	20
3 Log-Periodic Microstrip Antenna Design.....	23
3.1 Conventional LPMA Design for 5GHz – 8GHz Broadside Radiation	23
3.2 LPMA Design over the AMC Surface.....	25
3.2.1 Patch Antenna Design (model of the largest patch within the conventional LPMA)	26
3.2.2 AMC Design	27
3.2.3 Performance of the Patch Antenna over the AMC Surface	30
3.2.4 AMC Design for LPMA	34
3.2.5 Miniature AMC Based LPMA Performance	36
3.2.6 Comments on Design Limitations and Challenges	42
3.2.7 Experimental Verification.....	45
4 Conclusion	53
5 Future Work.....	54
References.....	55

List of Tables

Table 1: Size comparison between the traditional and the AMC based LPMA.....	41
Table 2: Broadside realized gain comparison between the traditional and AMC-based LPMA.....	42

List of Figures

Figure 1: Log-periodic dipole antenna with smaller end-loaded dipole elements.....	3
Figure 2: Log-periodic Koch dipole antenna	3
Figure 3: Conventional metallic vs. AMC ground plane	5
Figure 4: Basic configuration of an inset-fed microstrip patch antenna.....	7
Figure 5: Different metallization shapes employed in microstrip patch antenna design	8
Figure 6: Physical and effective length of rectangular patch antenna	9
Figure 7: Probe-fed patch antenna	11
Figure 8: Aperture-coupled feed.....	12
Figure 9: Proximity-coupled feed	12
Figure 10: Planar log-periodic antenna consisting of circular teeth	14
Figure 11: Log periodic dipole antenna	15
Figure 12: A printed log-periodic dipole antenna.....	16
Figure 13: Log-periodic microstrip antenna (actual design has 18 patches) [38].....	17
Figure 14: A 2-D EBG structure (this mushroom-like unit cell introduced by Sievenpiper [2])	18
Figure 15: LC model for mushroom EBG structure	19
Figure 16: Example of different metallization patterns employed in AMC unit cell design	22
Figure 17: LPMA with 11 square patches operating from 5GHz to 8 GHz (a) 3-D view (b) side view.....	24

Figure 18: (a) Return loss, and (b) input impedance performance of the designed LPMA	24
Figure 19: HFSS model of the square patch (33.77mm x 33.77mm).....	26
Figure 20: HFSS model for AMC unit cell design	28
Figure 21: (a) Magnitude and (b) Reflection phase of the AMC surface	29
Figure 22: After placing the AMC surface under the patch shown in Figure 19, new antenna resonate at 4.78GHz	30
Figure 23: 50% smaller patch over the AMC surface operates at 5.17GHz similar to the patch antenna shown in Figure 19.....	31
Figure 24: The return loss comparison of the conventional and AMC-based patch antenna	31
Figure 25: Simulated radiation pattern in $\phi=0$ (y-z plane cut).....	32
Figure 26: (a) Simulated return loss performance of the individual patch antennas that makes up the 11 element conventional LPMA, (b) Simulated return loss of 11 log-periodic scaled AMC-based miniature patch antennas.....	33
Figure 27: (a) AMC surface configuration #1. (b) AMC surface configuration #2	35
Figure 28: Simulated return loss of surface configuration #2 without radiating patches.....	36
Figure 29: (a) LPMA with AMC surface configuration # 1. (b) LPMA with AMC surface configuration # 2	37
Figure 30: Simulated return loss of the traditional and AMC-based LPMAs	37
Figure 31: Simulated input impedance of the AMC-based LPMA with surface configuration #1	38
Figure 32: Current distribution on the metallization of AMC-based LPMA with surface configuration #2 (a) 5GHz, (b) 6GHz, (c) 7GHz, (d) 8GHz	38
Figure 33: Simulated realized gain in y-z cut for (a) traditional LPMA, (b) with AMC surface configuration #1 (c) with AMC surface configuration #2.....	40
Figure 34: AMC based LPMA configuration #1 with 20mm substrate width	43

Figure 35: (a) AMC based LPMA configuration with fixed 0.4mm spacing metallic patch (b) Return loss performance of the LPMA on this AMC surface impedance.	44
Figure 36: Fabricated substrate layers of the traditional and AMC-based LPMA.....	45
Figure 37: The fabricated LPMA.....	46
Figure 38: The simulated and measured return loss of the traditional LPMA.....	47
Figure 39: The simulated and measured return loss of the AMC-based LPMA (configuration #1).	47
Figure 40: The simulated and measured return loss of the AMC-based LPMA (configuration #2).	48
Figure 41: Comparison between the measured return loss of the traditional LPMA and the AMC based LPMA with surface configuration #1 and #2.....	48
Figure 42: The simulated and measured broadside gains (a) Traditional LPMA (b) New LPMA with AMC surface 1 (c) New LPMA with AMC surface 2	49
Figure 43: Measured co-pol. gain pattern in the y-z cut (a) traditional LPMA (b) AMC-based LPMA configuration #1 (c) AMC-based LPMA configuration #2	50

Abstract

Microstrip patch antennas are attractive for numerous military and commercial applications due to their advantages in terms of low-profile, broadside radiation, low-cost, low-weight and conformability. However, the inherent narrowband performance of patch antennas prohibits their use in systems that demand wideband radiation. To alleviate the issue, an existing approach is to combine multiple patch antennas within a log-periodic array configuration [1]. These log-periodic patch antennas (LPMAs) are capable of providing large bandwidths (>50%) with stable broadside radiation patterns. However, they suffer from electrically large sizes. Therefore, their miniaturization without degrading the bandwidth performance holds promise for extending their use in applications that demand conformal and wideband installations.

In recent years, electromagnetic band gap structures have been proposed to enhance the radiation performances of printed antennas [2]. These engineered surfaces consist of a periodic arrangement of unit cells having specific metallization patterns. At particular frequencies, they provide a zero-degree phase shift for reflected plane waves and effectively act as high impedance surfaces. Since, their band-limited electromagnetic field behavior is quite similar to a hypothetical magnetic conductor; they are also referred to as artificial magnetic conductors (AMCs). AMC structures were shown to allow lower antenna profile, larger bandwidth, higher gain, and good unidirectional radiation by

alleviating the field cancellation effects observed in ground plane backed antenna configurations [3].

Previous research studies have already demonstrated that microstrip patch antennas can enjoy significant size reductions when placed above the AMC surfaces [4]. This project, for the first time, investigates the application of AMCs to LPMA configurations. Specifically, the goal is to reduce the LPMA size while retaining its highly desired large bandwidth performance. To accomplish this, we employ various AMC surface configurations (e.g. uniform, log-periodic) under traditional LPMAs and investigate their performance in terms of miniaturization, bandwidth, gain, and radiation patterns.

1. Introduction

The growing demand for broadband wireless communication systems continues to add more challenges for the design of RF device components. In military applications, conformal antennas with low profiles and small sizes are highly needed for platform installations. Patch antennas have been widely utilized in these types of applications, as they can operate within the close proximity of a ground plane with efficient broadband radiation. In addition, patch antennas have other attractive properties such as low cost, low weight and ease of fabrication. However, patch antennas are inherently narrow-band radiators and therefore they are useful for wideband communication systems. Although low permittivity ($BW \sim 1/\sqrt{\epsilon_r}$) and thick dielectrically substrates [5] can be applied to improve bandwidth, these methods increase the antenna weight and profile. Also, using a lossy substrate can alleviate some of the bandwidth issues at the expense of radiation efficiency.

To overcome the narrow band limitation, a log-periodic (LP) patch antenna configuration was proposed [5]. The idea is similar to the log-periodic trapezoidal or dipole antennas (originally introduced by DuHamel and Isbell in 1957) [6] that operate in free space with omnidirectional patterns. The wideband performance arises from the combined resonance effects of the multiple radiating elements that are arranged in logarithm scale of the frequency. Each element is responsible for radiating at a particular

band. This provides an overlapping radiation (i.e. frequency) response that covers the entire desired bandwidth [7].

As compared to the commonly employed omnidirectional antenna such as spiral antenna, the log-periodic microstrip antenna (LPMA) exhibits broadside radiation pattern which makes them attractive for military applications. Most importantly, LPMA operates over the same substrate thickness that a narrowband patch will utilize. Hence, it provides the low profile and wide bandwidth properties simultaneously. On the other hand, a printed spiral can also be designed to cover the same bandwidth with a smaller footprint. Nevertheless, such a spiral needs a relatively thicker substrate and introduces grating lobes when used in 1-D phased array configurations.

Generally speaking, log-periodic antenna configurations occupy a large physical area since multiple antenna elements having comparable size to half wavelength are combined to achieve the wideband radiation. To overcome this size disadvantage, many techniques have been investigated to miniaturize the traditional free-standing log-periodic antennas [8-13] (i.e. log-periodic antennas that are not radiating over ground plane). For example, a conventional log-periodic dipole antenna (LPDA) was miniaturized using small end-loaded dipole elements as shown in Figure 1. When the shape of the end-loaded dipoles and dimensions of the feed lines were optimized, this approach was shown to provide a 70% reduction in the LPDA size. In another study [9], different alignments of dipole antennas were investigated for size reduction. It was shown that a U-shape and straight line alignments (of radiating dipole elements) could lead to miniaturized LPDAs.

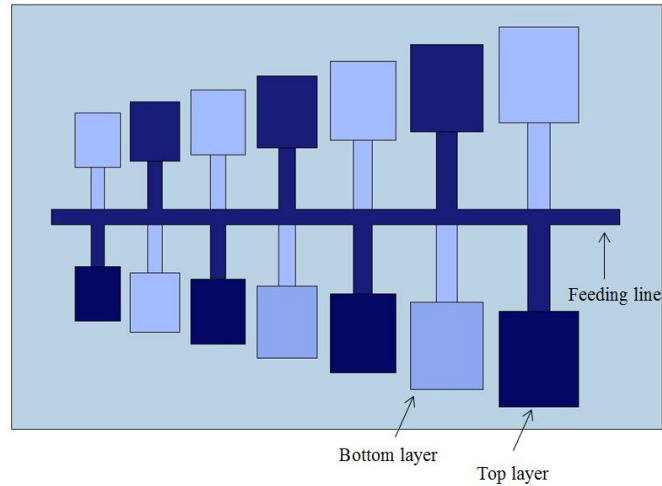


Figure 1: Log-periodic dipole antenna with smaller end-loaded dipole elements

A more recent miniaturization approach is to employ meandered lines as arms of the LPMA [10]. In addition, a Fractal or Koch technique can be applied as illustrated in Figure 2 [11-13]. The major goal of all these miniaturizing techniques is to accomplish size reduction without degrading the gain and radiation pattern performance throughout the whole operational band.

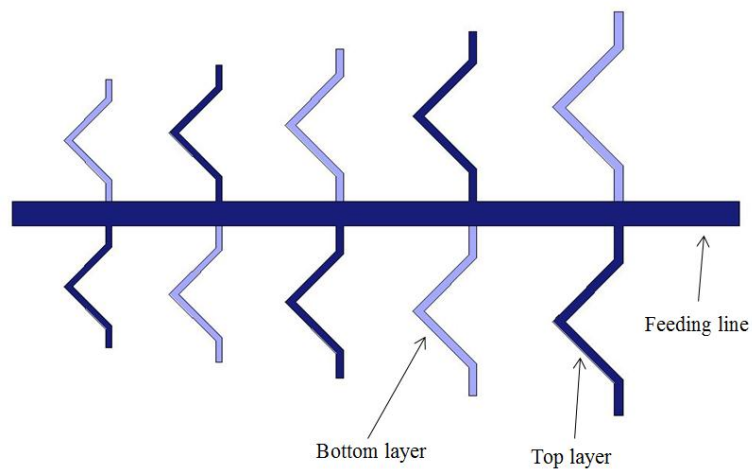


Figure 2: Log-periodic Koch dipole antenna

To the best of our knowledge, no miniaturization approach was undertaken for log-periodic microstrip patch antennas (LPMAs) that radiate within the close proximity of a ground plane. Therefore, the effort presented in this thesis represents the first of its kind. The design approach that will be investigated is based on miniaturizing the footprint of the individual patches within the LPMA by employing Artificial Magnetic Conductor surfaces or (reactive impedance surfaces). As will be shown, this design technique will allow the LPMA to maintain the same bandwidth performance with a 50% smaller footprint size without degrading the antenna profile.

Artificial Magnetic Conductor surfaces (AMC) are periodic structures that can provide a reflection response similar to a perfect magnetic conductor (PMC). This behavior is band-limited and the AMC surface acts like a regular metallic ground plane outside of its bandwidth. As shown in Figure 3, a conventional metallic ground plane reflects the electromagnetic waves with 180° phase shift ($\Gamma = -1$). On the other hand, the AMC surface can reflect the wave with zero degree phase shift ($\Gamma = +1$) at a particular band that can be controlled with its unit cell (i.e. the smallest building block of the periodic structure) parameters. When placed under a patch antenna, the AMC surface redistributes the image current in a way to reduce the mutual impedance between the antenna and its image. Therefore, another name for this structure is reactive impedance surface (RIS) [14]. Because of this property, the RIS can provide an increased bandwidth performance. In addition, the interaction between the antenna and the RIS has been shown to result in antenna miniaturization and increased front to back radiation ratio [14-19].

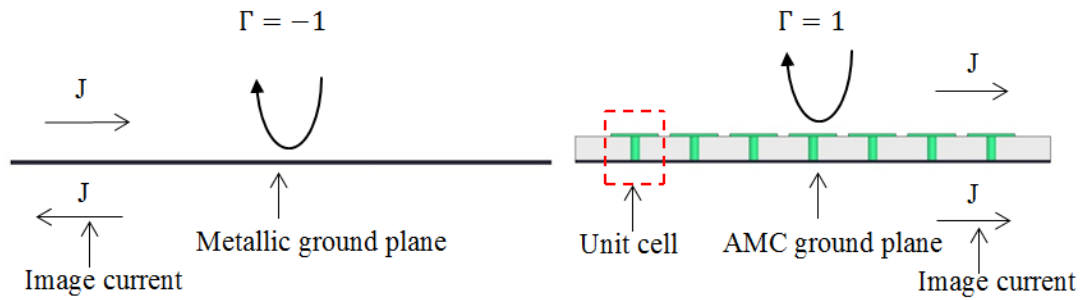


Figure 3: Conventional metallic vs. AMC ground plane

The bandwidth of the AMC, in general, is defined as the frequency range where the phase of the reflection coefficient changes from -90° to $+90^\circ$. At the center frequency, the AMC surface provides a zero phase reflection coefficient. The geometrical parameters of the AMC unit cell control the operation frequency and bandwidth. Many different shapes have been proposed and studied to improve the bandwidth performance of the AMC cells in recent literature [20-26]. AMC surfaces have been proposed to improve performance of many antenna configurations, such as dipoles [19] and patches [23]. In addition, they are proposed as ground plane substrates of textile and flexible antennas [27] that are operating at lower frequencies [28-29]. AMC surfaces were also investigated as alternative low profile antenna ground plane [30]. Microstrip slot antennas were also shown to benefit from AMC surfaces in term of efficiency and were employed in phased array configurations [31-32].

As mentioned before, our goal is to investigate miniaturization of LPMAs using AMC surfaces. In the following section, we summarize the commonly employed microstrip patch antenna configurations and demonstrate the existing feeding techniques with their advantages and disadvantages. Section 2.2 demonstrates the design principles

of traditional LP and LPMAs. In section 2.3, we present a background in modeling and design of the AMC unit cells for specific antenna applications. Section 3.1 presents a LPMA design that operates from 5GHz to 8 GHz. The following section describes the design approaches taken to miniaturize the LPMA using the AMC surface. Specially, in section 3.2.4, we present a 50% smaller LPMA design that operating with the same bandwidth and antenna profile performance to that of the conventional design. Section 3.2.7 presents a performance comparison between simulated and fabricated antennas. The conclusion and future work are discussed in sections 4 and 5, respectively.

2. Background and Literature Review

2.1. Microstrip Patch Antennas and Design Principles

Figure 4 depicts a basic configuration of an inset-fed rectangular patch antenna. As seen, the antenna consists of a metalized pattern over a thin microstrip substrate. The back surface of the substrate is utilized as ground plane. Typically, the length of the patch (L) is about $\lambda_g/2$ (where λ_g is the effective wavelength) and the substrate thickness (h) is in the order of $\sim \lambda_g/20$. Due to the $\lambda_g/2$ spacing between the radiating slots and the presence of the ground plane metallization, the main power radiated from the patch is oriented towards z axis. This is also referred to as broadside radiation.

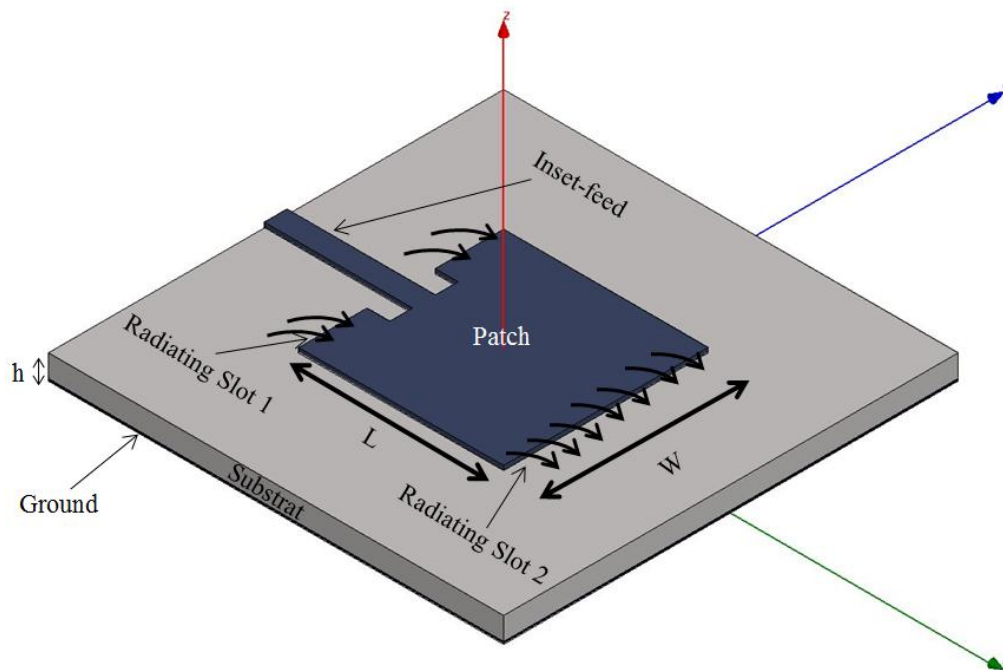


Figure 4: Basic configuration of an inset-fed microstrip patch antenna

The thickness and the relative permittivity of the substrate are the most critical parameters in controlling the bandwidth, efficiency, and radiation pattern of the patch antenna. The radiating patch can also be made in different geometric shapes as illustrated in Figure 5. In certain patch antenna designs, the location and the number of feeds can be utilized to achieve a particular polarization state (e.g. linear, circular, etc.). An array of multiple patches also can be used to construct a phased array in order to direct the beam to a desired direction.

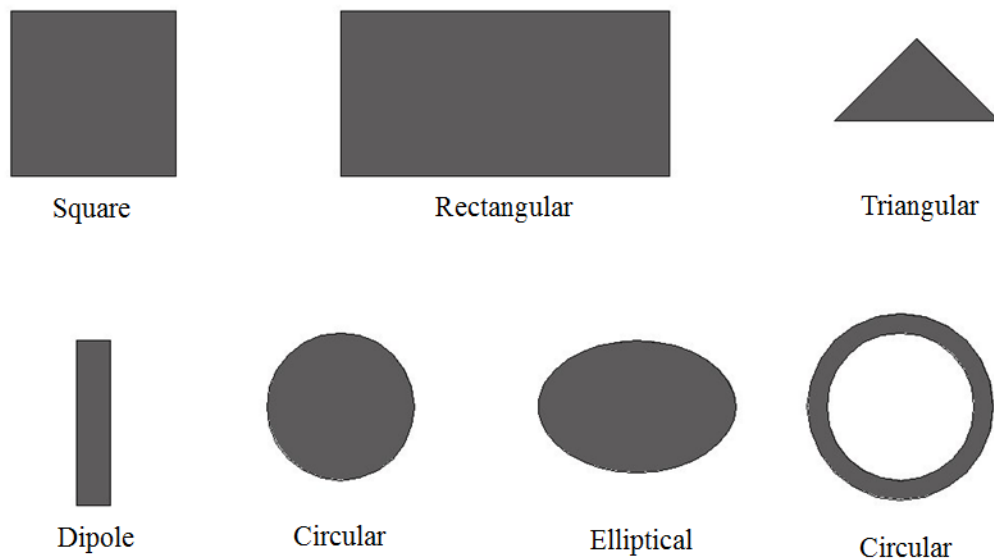


Figure 5: Different metallization shapes employed in microstrip patch antenna design

Due to the finite size of the radiating patch, the field distributions at the radiating apertures are not uniform and fringes as shown in Figure 6. Hence, the fringing fields effectively increase the length of the patch (by ΔL) and need to be accounted in determining the resonance frequency. The most commonly used design equations that

take the fringing field into account can be found in many text books [33] and presented below for completeness.

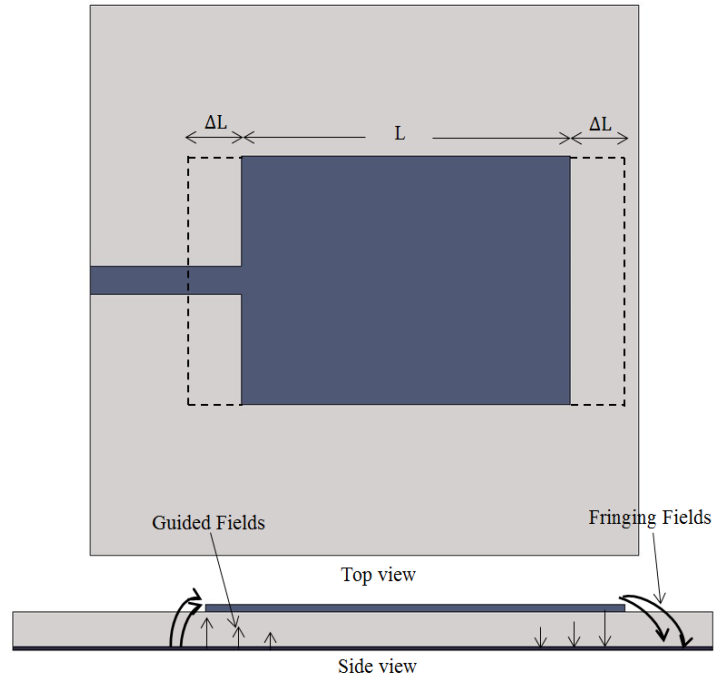


Figure 6: Physical and effective length of rectangular patch antenna

In patch design, first an effective dielectric constant should be calculated from [33]:

$$\epsilon_{r_{eff}} = \frac{\epsilon_r + 1}{2} + \frac{\epsilon_r - 1}{2} \left[1 + 12 \frac{h}{W} \right]^{-1/2}$$

$$W/h > 1$$

to take into account the finite thickness of the substrate material. Next, an effective length, width and resonant frequency equations can be utilized successively to complete the design:

$$\Delta L = 0.412 h \frac{(\epsilon_{reff} + 0.3) \left(\frac{W}{h} + 0.264\right)}{(\epsilon_{reff} - 0.258) \left(\frac{W}{h} + 0.8\right)}$$

$$L_{eff} = L + 2\Delta L$$

$$(f_r)_{010} = \frac{1}{2L_{eff}\sqrt{\epsilon_r}\sqrt{\mu_0\epsilon_0}}$$

$$W = \frac{2}{2f_r\sqrt{\mu_0\epsilon_0}} \sqrt{\frac{2}{\epsilon_r + 1}}$$

$$L = \frac{1}{2f_r\sqrt{\epsilon_{reff}}\sqrt{\mu_0\epsilon_0}} - 2\Delta L$$

Many different feeding techniques exist for patch antennas. The most general methods can be summarized as below:

2.1.1. Microstrip Line Inset-Feed

As shown in Figure 4, the inset-feed is easy to fabricate as it is implemented on the same substrate surface that accommodates the radiating patch. The width of the line is small as compared to that of the patch. The overall widths also vary and needs to be designed for different thickness and permittivity values of the substrate. This feeding technique is not practical for thick substrates and limits the bandwidth by 2% to 5% [33].

2.1.2. Coaxial-Probe

This method employs coaxial cable by connecting the inner conductor to the proper location in the radiating patch. The outer conductor of the cable is connected to the ground plane as shown in Figure 7. The performance of this feed technique is similar

to that of the inset-feed technique. It provides a narrow bandwidth performance and it is difficult to design for thick substrates [33].

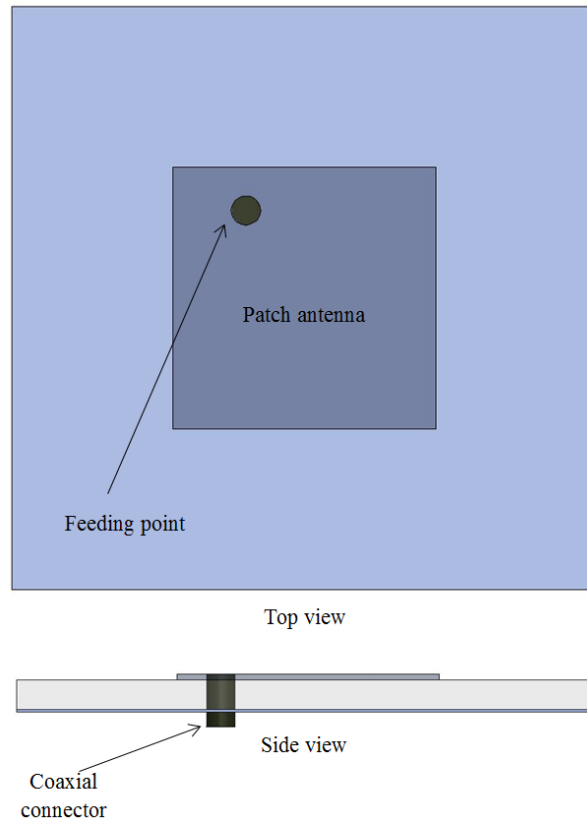


Figure 7: Probe-fed patch antenna

2.1.3. Aperture-Coupled Feed

The previous two techniques are usually vulnerable to produce higher order mode excitations that can affect the radiation of the antenna. An aperture-coupled feed is found attractive for this reason. However, this technique is also for narrow band patch antennas. In addition, the feed layout is difficult to design and fabricate. As shown in Figure 8, two substrates with microstrip feed line printed on the bottom one and the radiating patch printed on the top one are employed. An aperture shape is placed under the radiating patch in order to control the coupled energy from the microstrip line [33].

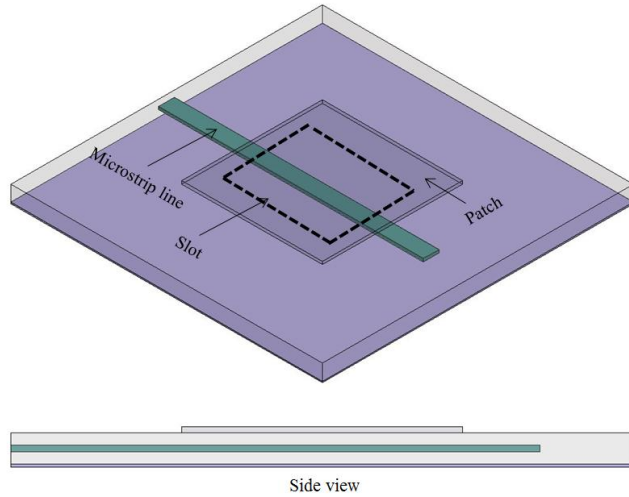


Figure 8: Aperture-coupled feed

2.1.4. Proximity-Coupled Feed

This technique provides a wider bandwidth (up to 13%) and low spurious radiation as compared to the previous techniques. It consists of two substrates where the top one carries the radiating patch whereas the bottom one has the feed line [5] as shown in Figure 9. The line can be matched by controlling its length and width as well as its relating position with respect to the radiating patch [33].

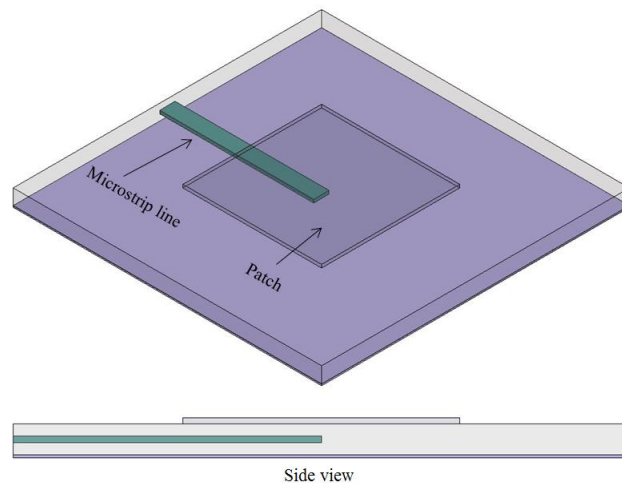


Figure 9: Proximity-coupled feed

2.2. Log-Periodic (LP) Antennas

The Log-periodic antenna shown in Figure 10 was first introduced by DuHamel and Isbell [6]. They categorized this antenna as frequency independent providing bandwidth greater than 10:1. To obtain a uniform radiation behavior throughout the wide bandwidth, the geometrical parameters of the antenna sectors must be logarithmically scaled. The antenna in Figure 4 is linearly polarized and provides bi-directional radiation pattern. Specifically, the LP antenna geometry is defined using a transformation equation as:

$$z = \ln(w)$$

where $z = x + jy$ (rectangular coordinate) and $w = \rho e^{j\theta}$ (cylindrical coordinates). This transformation can also be written as:

$$\rho = e^x \text{ or } x = \ln(\rho)$$

$$\theta = y .$$

The name “log-periodic” comes from the uniform spacing between the resonance frequencies of the antenna when plotted in a logarithmic scale. As shown in Figure 10, the first log-periodic planar antenna consisted of circularly curved teeth with different lengths. The tooth length and the distance from the center increases periodically with ratio:

$$\tau = \frac{R_n}{R_{n+1}} .$$

Consequently, τ represents the ratio between two adjacent resonance frequencies as:

$$\tau = \frac{f_1}{f_2} \quad f_2 > f_1$$

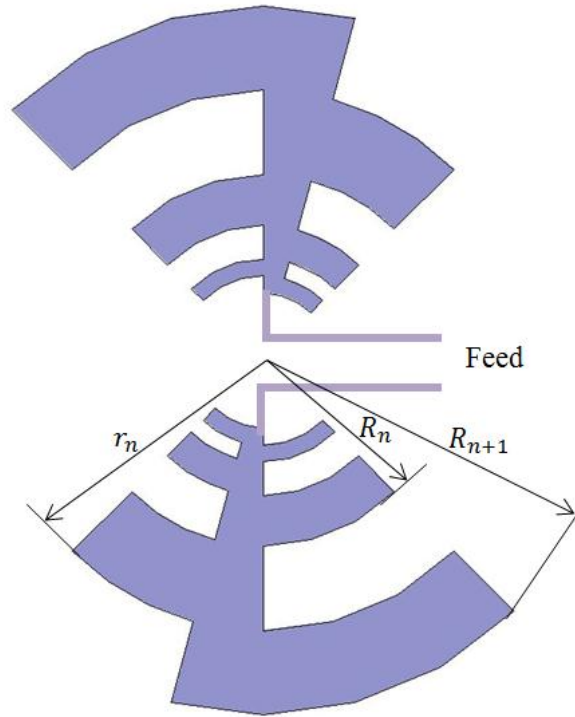


Figure 10: Planar log-periodic antenna consisting of circular teeth

To provide a uniform radiation performance, τ (expansion ratio) must be selected small enough. The size of the smallest teeth determines the highest resonance frequency (f_H), whereas the size of the largest teeth identifies the lowest operational frequency (f_L). Each tooth provides a resonance frequency between f_L and f_H , corresponding to its individual size. The LP antenna is fed from the high frequency end in order to prevent the lower frequency content being radiated from the higher order modes of the largest teeth.

Another popular LP antenna configuration is the dipole array (LPDA) as shown in Figure 11. LPDA resembles a Yagi-Uda antenna in design, but operates with a significantly different perspective. The Yagi-Uda antenna has 1 radiator with many parasitic elements; however all of the dipole elements in LPDA are responsible for radiation at particular frequencies [34]. Hence, LPDA can provide much broader

bandwidth. The LPDA elements are often fed with 180° phase shift to produce an end-fire pattern [35]. A feeding approach is to use a broadband balun connected between two end terminals of the feeding line. Since it is difficult to apply the LP techniques to the feed line; uniform wires are used for implantation. This feeding also provides better impedance match by minimizing the near field-interaction between the adjacent elements.

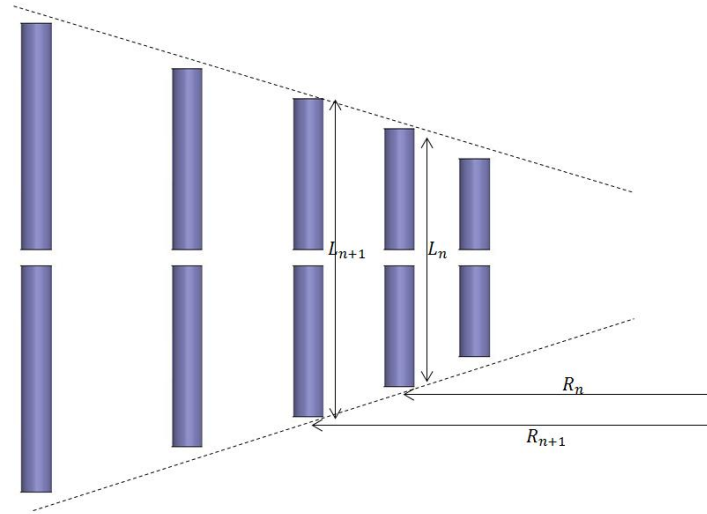


Figure 11: Log periodic dipole antenna

Similar to the LP antenna with circularly curved teeth, the smallest cutoff frequency of the LPDA is related to the resonance frequency of the longest element when its length becomes comparable to $\lambda/2$. Likewise, the largest cutoff frequency depends on the resonance frequency of the smallest element. To operate at particular band, a portion of the LP antenna geometry should have a resonant feature size to provide radiation.

LPDAs can also be conveniently fabricated on printed microstrip substrates [39]. In [39], a 12 element LPDA radiating from 1 to 2 GHz was demonstrated using 0.794mm thick $\epsilon = 2.45$ substrate. The antenna was fed using a balun configuration. In this

approach, the top surface of the substrate carries the half of the dipoles and the bottom surface carries the other half as shown in Figure 12.

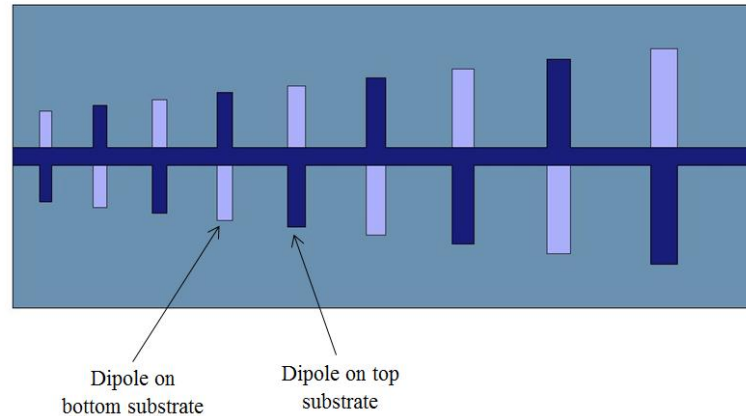


Figure 12: A printed log-periodic dipole antenna

Due to the low profile, low weight and conformability of the patch antenna, log-periodic microstrip patch antennas (LPMAs) were also introduced to overcome the narrow band of a single patch antenna. The LPMAs can be fed using the same techniques as a single patch antenna. Among the different techniques that have been investigated, quarter wavelength line-coupled, comb-line array and series connected patch array [36] were all shown to introduce a stop-band in the region of operation; thus inhibiting wideband performance. On the other hand, a coupled overlaid patch array (i.e. proximity fed) was shown to produce a wideband radiation without introducing any stop-bands, because a capacitive coupling between the feeding line and the radiating patches were utilized instead of direct contact. Aperture coupling techniques were also proven to be useful in LPMA design [37].

Figure 13 demonstrates a proximity fed LPMA design that was presented in [38]. The LPMA has a 50Ω microstrip line feed on the bottom substrate coupled to 18

rectangular patches printed on the top substrate with metallic ground plane. The electromagnetic coupling from the feed line to the patch is determined by the thickness of the substrate and the relative location of the patch with respect to the feed line. This LPMA achieved about 10dB gain on 1mm thick, $\epsilon_R = 2.5$ substrate with 150mm x 50mm substrate size. The antenna radiated from 8GHz to 18 GHz, and an expansion factor of $\tau = 1.05$ was utilized.

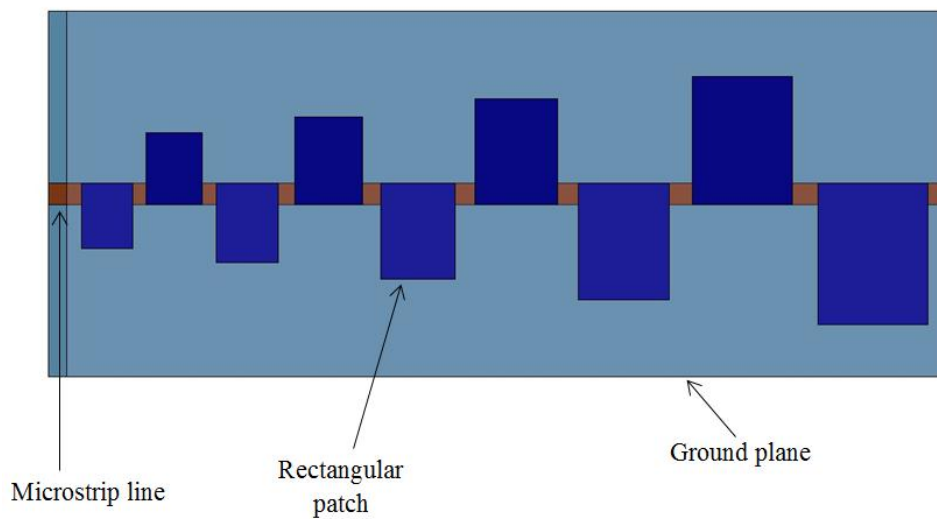


Figure 13: Log-periodic microstrip antenna (actual design has 18 patches) [38]

Analytical model for planar LPMA has been derived [40] to calculate the number and the location of resonance frequencies. A single layer LPMA was presented in [41]. It consisted of patch antennas arranged in each side of a microstrip feed line. The feed line was on the same surface with the antennas. 11 antenna elements with $\tau=1.1$ were used to radiate from 2.26GHz to 6.25GHz. This LPMA had a physical size of 320mm x 110mm.

2.3. Artificial Magnetic Conductor (AMC) and Electromagnetic Band Gap (EBG) Structures

AMC and EBG structures are periodic assemblies of unit cells that are composed of a geometrical arrangement of readily available materials (such as dielectrics, conductors, etc.). Due to the periodicity and electromagnetic interactions among the unit cells, these structures can exhibit unique properties that cannot be found in any of their bulk individual constituents. For example, at particular frequency ranges, EBG structures prevent the propagation of electromagnetic waves in certain directions. Due to this property, 2-D EBG structures (see Figure 14) are often employed to enhance the radiation performances of the patch antennas by suppressing the surface wave propagation. Likewise, AMC surfaces can reflect incident electromagnetic waves without any phase shift at particular frequency regions.

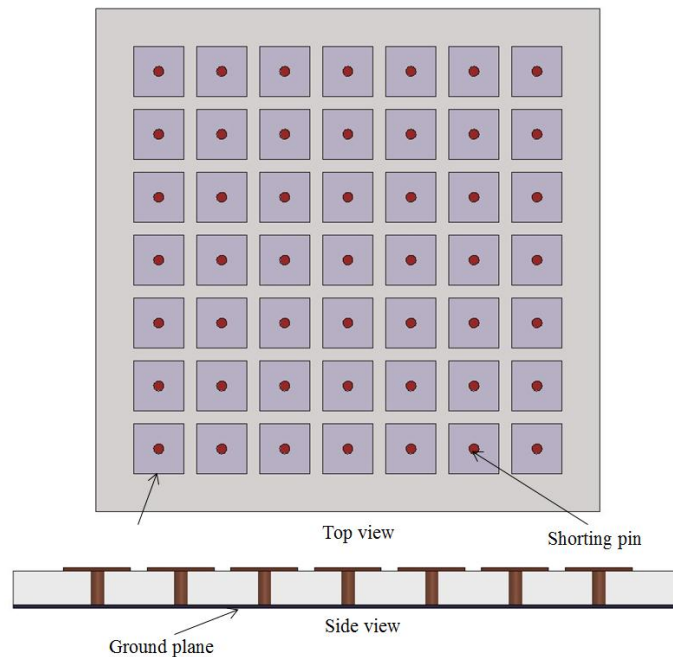


Figure 14: A 2-D EBG structure (this mushroom-like unit cell introduced by Sievenpiper [2])

A 2D EBG structure can also act as an AMC surface when being operated at their band-gap frequencies. On the other hand, an AMC surface configuration does not necessarily display a band-gap property. To design the EBG/AMC structures, two different models are generally utilized by different research groups. These models are named as [42]:

a) Lumped element, and b) full wave computational. In the following subsection, we will briefly explain these models:

2.3.1. Models for Designing EBG/AMC Unit Cells

2.3.1.1. The Lumped Element Model

This model is the simplest among all others. The unit cell is modeled as a lumped circuit consisting of capacitors and inductors. For the mushroom type unit cell introduced by Sievenpiper in 1999[2] (this unit cell is the most commonly employed EBG configuration shown in Figure 15):

$$C = \frac{W\epsilon_0(1 + \epsilon_r)}{\pi} \cosh^{-1}\left(\frac{W + g}{g}\right)$$

$$L = \mu h$$

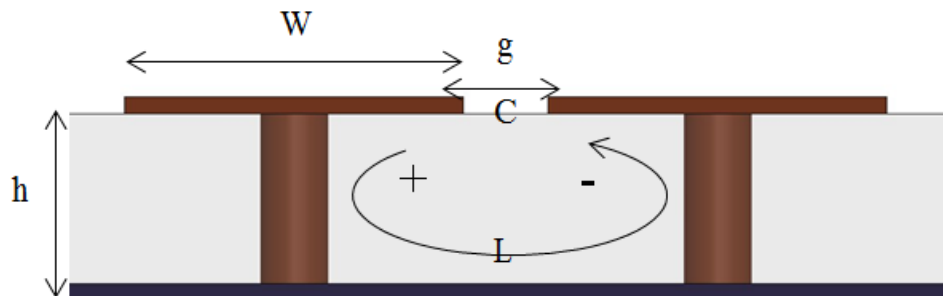


Figure 15: LC model for mushroom EBG structure

where C represents the capacitance between each adjacent AMC unit cell, W is the width of the metallic patch, g is the gap between the unit cell and h represent the height of the patch from the conventional ground plane. The EBG structure inhibits surface wave propagation at the resonance frequency of $\omega = 1/\sqrt{LC}$. As can be seen, this method does not give much information about bandwidth and dissipation of the electromagnetic energy.

2.3.1.2. Full Wave Numerical Modeling

This technique gives an accurate result not only for mushroom-like EBG unit cell but for any other type of unit cell layout. It can also be utilized to obtain other important information such as reflection phase from multiple angles of incidence, dispersion diagram for various propagation directions, surface impedance observed by the incident field, and the frequency bandwidth of the band-gap region. This method is already implemented in commercially available electromagnetic softwares (such as Ansoft AFSS) and makes use of the periodic boundary conditions. These boundaries ensure that the EBG unit cell is accurately modeled inside an infinitely large periodic assembly. An incident wave can be defined and transmitted toward the center of the EBG cell to calculate the amplitude and phase of the reflected wave.

2.3.2. EBG/AMC Structures in Antenna Applications

A common application of EBG structures pertains to improve the polarization state and radiation pattern of a planar antenna radiating over a large ground plane. This is achieved by employing the EBG substrate around the antenna to suppress undesired

diffraction-based radiation due to the surface wave. This, in turn, enhances the antenna gain and efficiency. The same principle of surface wave suppression also finds application for reducing the mutual coupling between two adjacent antennas within a phased array [25-29].

Wire antennas [44] can be used as efficient low profile radiators when employed over the EBG structures. Because of the image theory, a conventional wire antenna cannot be placed very near to the ground plane. Since, the ground plane reflects the waves radiated by the wire antenna with 180° phase shift; the reflected wave interferes destructively with the direct radiation. On the other hand, the EBG structure acts as an AMC in its band-gap frequency, and reinforces radiation creating by an in-phase reflected wave. This mechanism improves the gain, efficiency and bandwidth of the low profile wire antennas.

AMC surface is quite similar to an EBG structure and it can be fabricated as a metallic patch on top of a grounded dielectric material. As compared to the mushroom-like EBG, AMC unit cell does not need a shorting pin. Thus, AMC unit cell does not exhibit a band-gap but still reflects the incident waves with zero degree phases. It also acts as a high impedance surface redistributes the surface current in a way that it can enhance the antenna performance [45-49] (hence referred to as a reactive impedance surface by some others [45]). Typically, when used as patch antenna ground planes, both EBG and AMC structures reduces the resonance frequency down. Therefore, they also result in size reduction.

The metallic part in the AMC cell can be designed to take different geometrical shapes [3] and [43] as shown in Figure 16. The reflection coefficient from the AMC

surface varies with the incident angle and significantly changes beyond 30° from the normal.

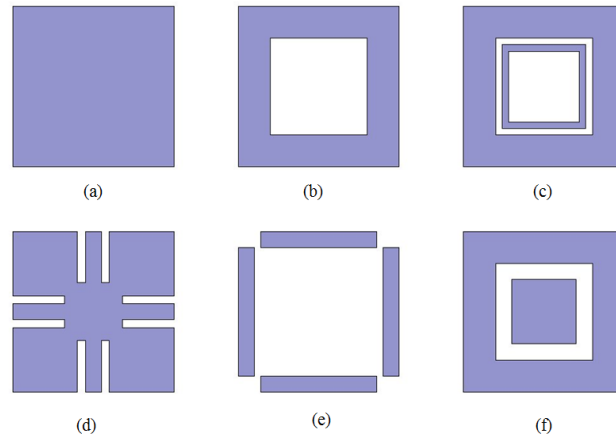


Figure 16: Example of different metallization patterns employed in AMC unit cell design

Multiband AMC surfaces can be designed using multi-layered AMC surfaces resonating at different frequencies. For example in [50], zero reflection phases were achieved at two frequency bands (850MHz and 1900MHz) by using dual AMC surfaces. Another approach is to use an optimization algorithm to design the unit cell layout to cover multiple bands. In [51], an increase in the bandwidth from 31% to 81% was achieved in a tri-band AMC surface using genetic algorithm. Tunable multiband AMC surfaces were also investigated by integrating diodes among the metallic patches. For instance in [52], the AMC was designed to operate at two particular frequencies by using the on/off state of the diode. Another multiband design operating at 2.4, 4.5, 5.2, and 5.8GHz were designed using multilayer substrates [53].

3. Log-Periodic Microstrip Antenna Design

Traditionally log-periodic microstrip antenna occupies a large size on a single substrate. In this section, we detail our design approach for miniaturizing the LPMA using AMC surfaces. Specifically, we consider a LPMA configuration operating from 5GHz to 8GHz with $|S_{11}| < -10\text{dB}$ return loss.

3.1. Conventional LPMA Design for 5GHz – 8GHz Broadside Radiation

To cover the entire bandwidth from 5GHz – 8GHz, 11 patches with scaling factor of $\tau = 1.07$ was needed. Figure 17 demonstrates the LPMA that was modeled in HFSS v12. Both substrates are identical with $\epsilon_r = 2.94$, $\tan \delta = 0.0012$, and thickness of 1.524mm. The bottom surface of the bottom substrate is utilized as ground plane and the overall antenna thickness is 3.048mm. The patch radiators of the LPMA occupy 23.63mm x 114.63mm footprint area and the substrate size is 50mm x 122.5mm, with 12.7mm separation between the edge of the largest patch and the substrate edge. At any given frequency within 5GHz – 8GHz, there is at least one patch radiating in broadside direction. The largest patch has dimensions of 13.77mm x 13.77mm and responsible for 5GHz radiation. As shown in Figure 18, the LPMA is well matched (i.e. $|S_{11}| < -10\text{dB}$) above 4.9GHz. Although the impedance maintains matching above 8GHz, the radiation beyond this frequency is mainly due to the higher order modes. As seen in Figure 18, the pattern is significantly tilted away from the broadside direction. Hence, the useful pattern

bandwidth is up to 8GHz which is determined by the 7mm x7mm size of the smallest patch in the LPMA configuration.

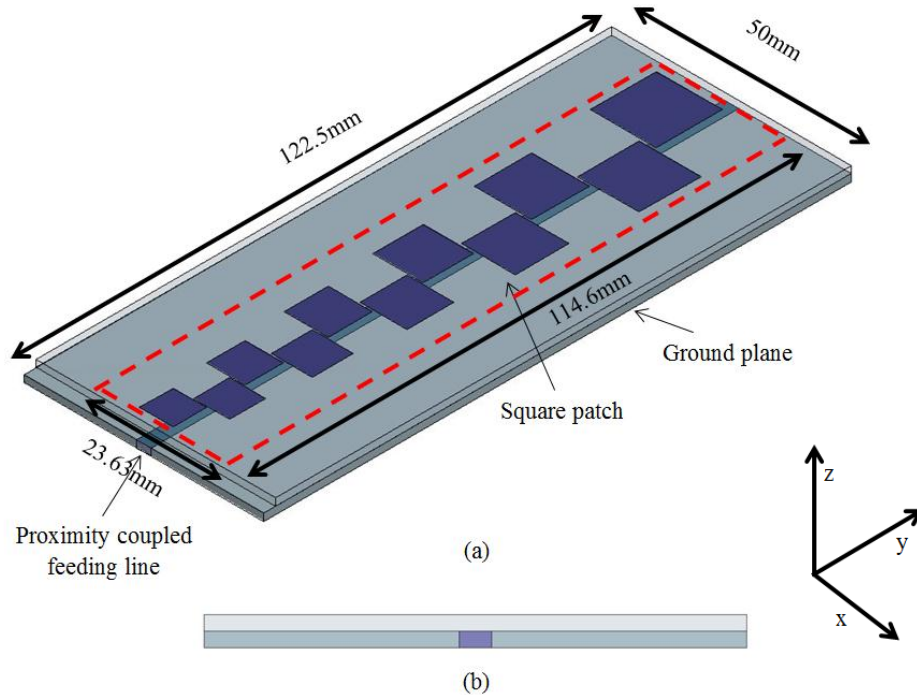


Figure 17: LPMA with 11 square patches operating from 5GHz to 8 GHz (a) 3-D view
(b) side view

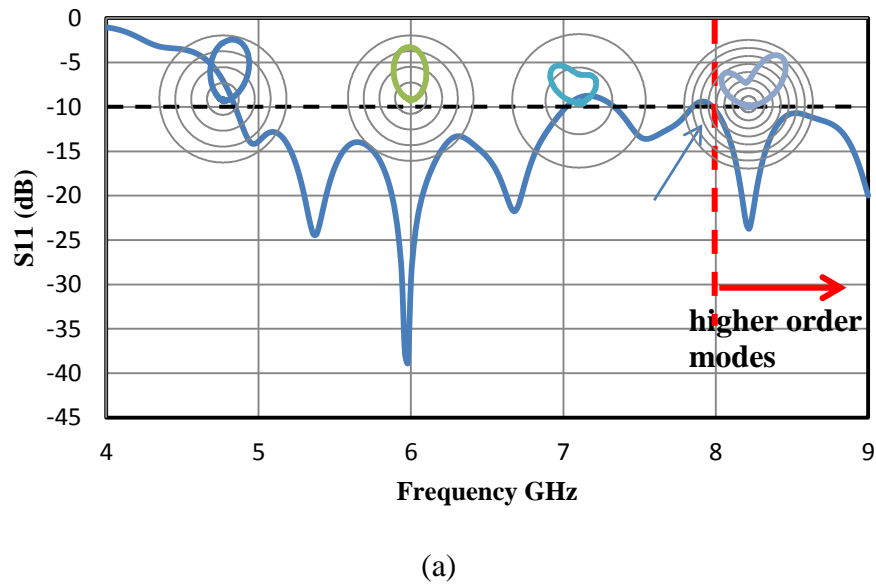
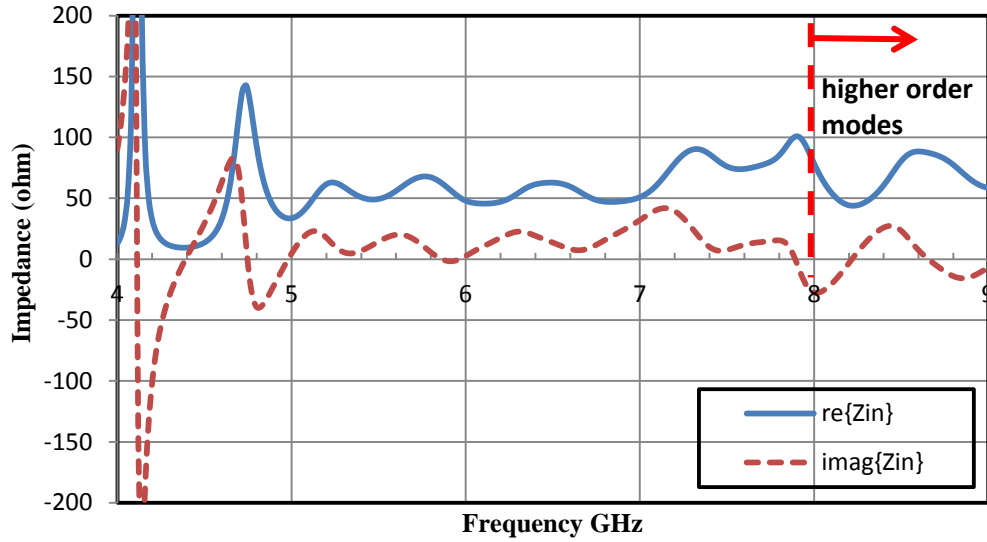


Figure 18: (a) Return loss, and (b) input impedance performance of the designed LPMA



(b)

Figure 18: (continued)

3.2. LPMA Design over the AMC Surface

Our design starts by considering a single patch antenna element of the conventional LPMA design. For simplicity, we selected the largest patch and reduced its thickness by half (down to 1.524mm) to accommodate the AMC surface without increasing the overall substrate thickness. Next, a square AMC unit cell providing zero degree phase shift at the resonance of the thin patch antenna was designed. Specifically, since the thinner patch exhibited its resonance at 5.96GHz (as compared to 5.17GHz of the 3mm thick patch) the AMC was designed to operate at this frequency. Subsequently, several AMC unit cells were placed under the antenna to harness its electromagnetic properties. Consequently, the combined (i.e. antenna and AMC surface) geometry was found to exhibit a resonance at a much lower frequency of 4.78GHz. To bring the resonance back to the same frequency of the original 3mm patch, the antenna footprint

over the AMC surface was scaled down by about 50%. Hence, the AMC surface was found to provide a 50% smaller footprint as compared to that of the conventional patch antenna.

Having completed the AMC-based patch design, 11 such elements were logarithmically scaled with respect to each other and brought together to form LPMA configuration. Below we detail our design approach starting from the design of the single patch.

3.2.1. Patch Antenna Design (model of the largest patch within the conventional LPMA)

Figure 19 shows the largest patch of the conventional LPMA. The antenna has footprint of 13.77mm x 13.77mm over a 3.048mm thick $\epsilon_r=2.94$ substrate. It resonates at 5.17GHz with 400MHz bandwidth.

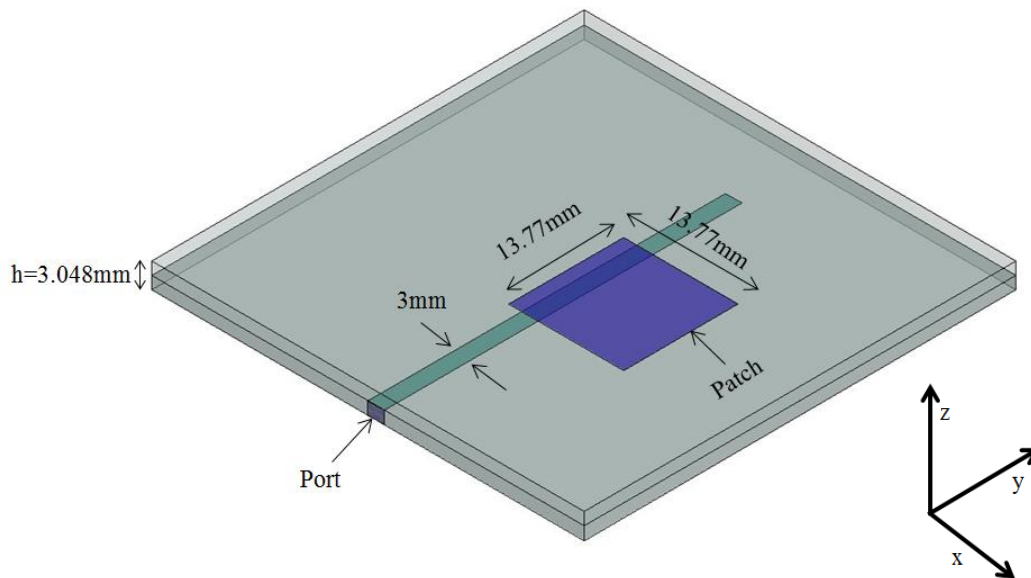


Figure 19: HFSS model of the square patch (33.77mm x 33.77mm)

To maintain the same thickness after adding on AMC layer, we reduced the thickness of this patch down to 1.524mm. This thickness shifts the resonance frequency up to 5.96 GHz with 160MHz bandwidth. As will be shown in the following sections, the interaction with the AMC surface will shift this resonance well below the original frequency of 5.17GHz and eventually result in antenna miniaturization.

3.2.2. AMC Design

The AMC unit cell consisting of a printed square patch was designed in HFSS using the periodic boundary conditions as shown in Figure 20. The overall size of the unit cell is 4.9mm x 4.9mm and the patch has dimensions of 4.5mm x 4.5mm. Due to the capacitive coupling between the adjacent unit cell patches, increasing the AMC patch size decreases the zero phase reflection frequency. Likewise, smaller patch sizes within the 4.9mm unit cell result in higher operational frequencies. For the LPMA, special attention must be given to employ miniature AMC unit cells. The size of the AMC cell cannot be equal or greater than the radiating patches, because the AMC metallization will get excited by the feed line similar to an antenna. To miniaturize the AMC unit cells, we chose a high permittivity substrate with $\epsilon_r = 10.2$ and thickness of 1.27mm. This selection insured that the AMC unit cells were smaller than the smallest radiator patch within the LPMA configuration.

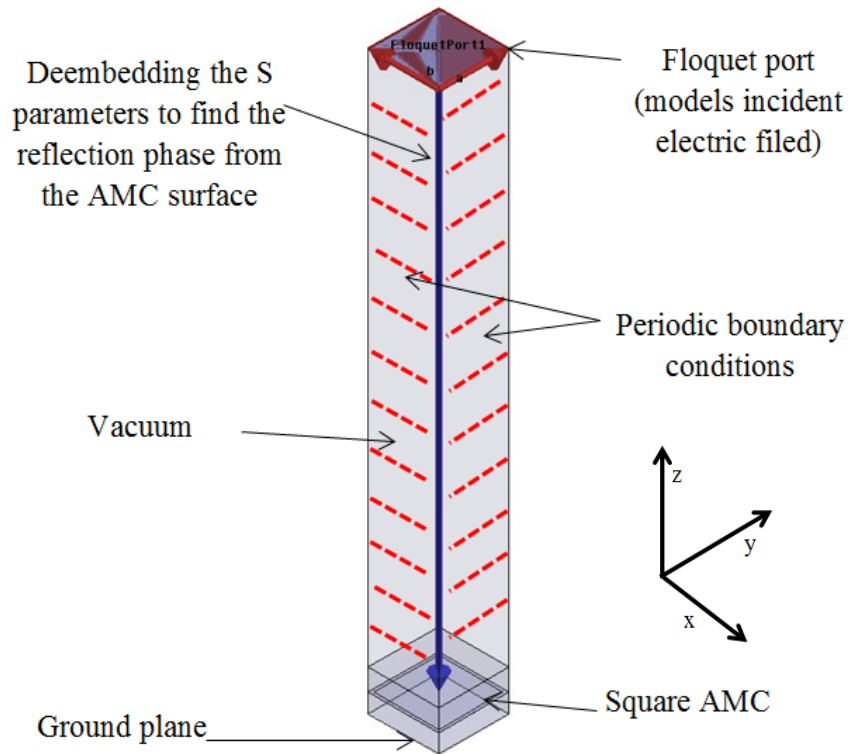
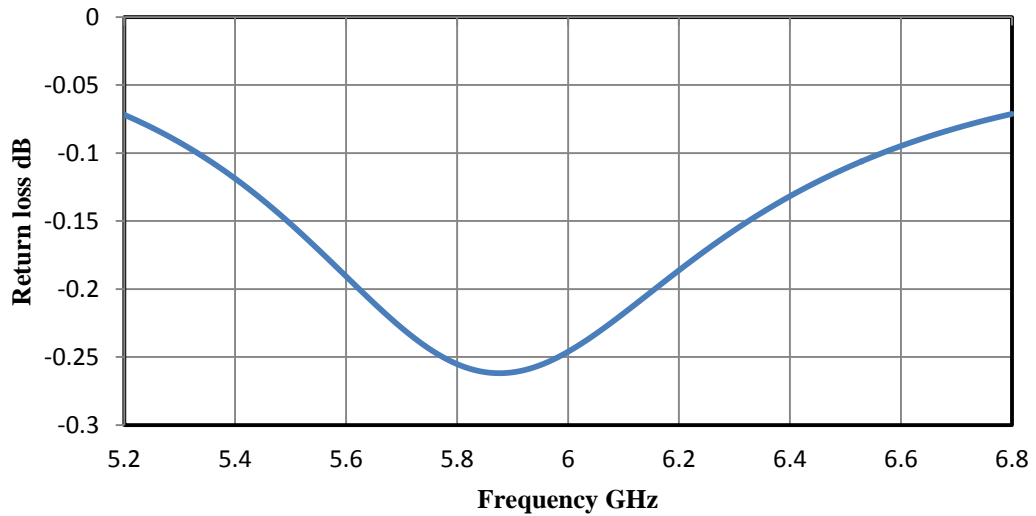


Figure 20: HFSS model for AMC unit cell design

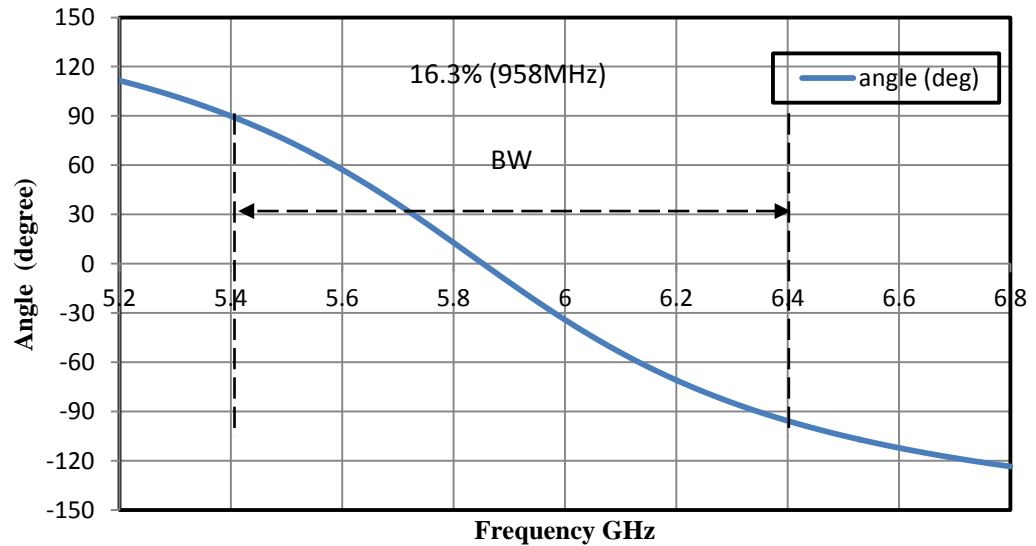
As shown in Figure 21, the designed AMC exhibits a zero phase reflection with a -90° to $+90^\circ$ bandwidth of 958MHz for normally incident wave. This band covers the operational bandwidth of the 1.524mm thick antenna that was demonstrated in the previous section. The bandwidth of the AMC cell depends on the thickness of the substrate. As the thickness of the substrate increases, the bandwidth becomes wider. From the magnitude of the reflection coefficient depicted in Figure 21(a), one can conclude that the AMC surface will absorb $\sim 5\%$ of the incident power due to the metallic and dielectric loss.

An AMC surface having unit cells with a patch size of 2.1mm x 2.1mm has been used for the smallest patch of the traditional LPMA (with 1.524mm thickness and a

resonance frequency of 10.2GHz). Since a patch that will be placed over the AMC surface will not generate all normally incident fields, the antenna efficiency should be reduced less than (5%) due to the presence of this AMC surface.



(a)



(b)

Figure 21: (a) Magnitude and (b) Reflection phase of the AMC surface

3.2.3. Performance of the Patch Antenna over the AMC Surface

Having completed the AMC unit cell design, we proceeded by placing arrangements of the 5x5 AMC unit cell arrangement under the patch antenna. The 1.27mm thick AMC unit cells are positioned to cover the entire footprint of the patch as shown in Figure 22. The new antenna design uses three substrate layers with an overall thickness of 2.794mm (i.e. top layer for the patch, middle layer for the feed and bottom layer for the AMC). Due to the interaction between AMC surface and the patch antenna, the resonance frequency shifts from 5.96GHz down to 4.78GHz. The antenna exhibits 4.6% $|S_{11}| < -10\text{dB}$ bandwidth (i.e. 220MHz). To shift the resonance of the antenna up to 5.17GHz (i.e. resonance frequency of the largest patch in the traditional LPMA design, see Figure 18), size of the patch was scaled down by 50% without changing the AMC unit cell size (see Figure 23). As compared to the 5.17GHz patch on 3.048mm thick $\epsilon_r=2.94$ substrate, the new patch design with the AMC surface exhibits a larger bandwidth (see Figure 24) ($S_{11}<-10\text{dB}$) despite being 50% smaller and utilizing a lower 2.794mm profile over the ground plane.

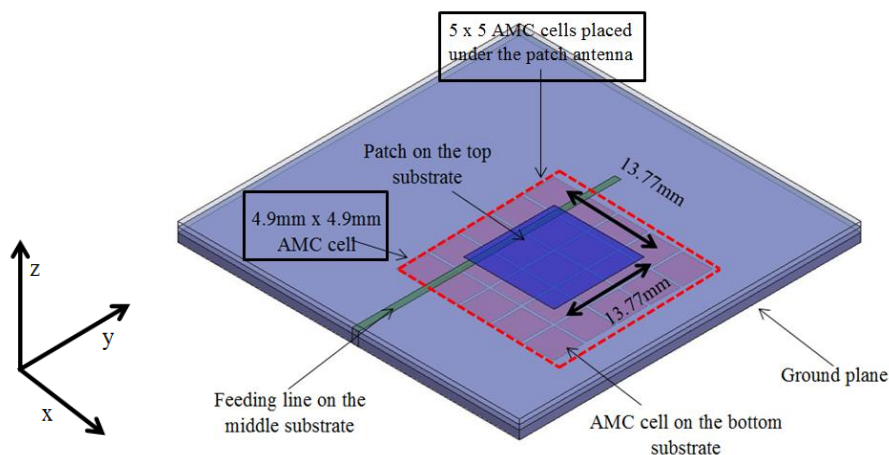


Figure 22: After placing the AMC surface under the patch shown in Figure 19, new antenna resonate at 4.78GHz

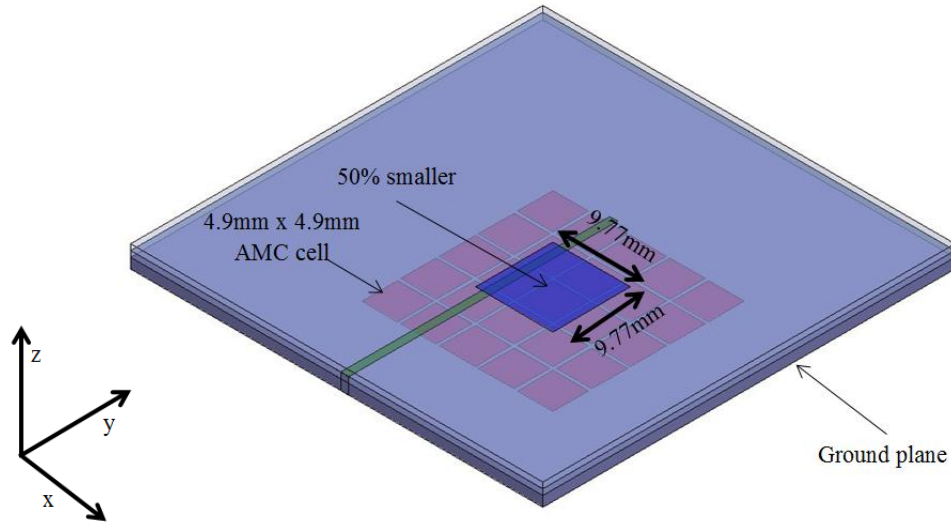


Figure 23: 50% smaller patch over the AMC surface operates at 5.17GHz similar to the patch antenna shown in Figure 19

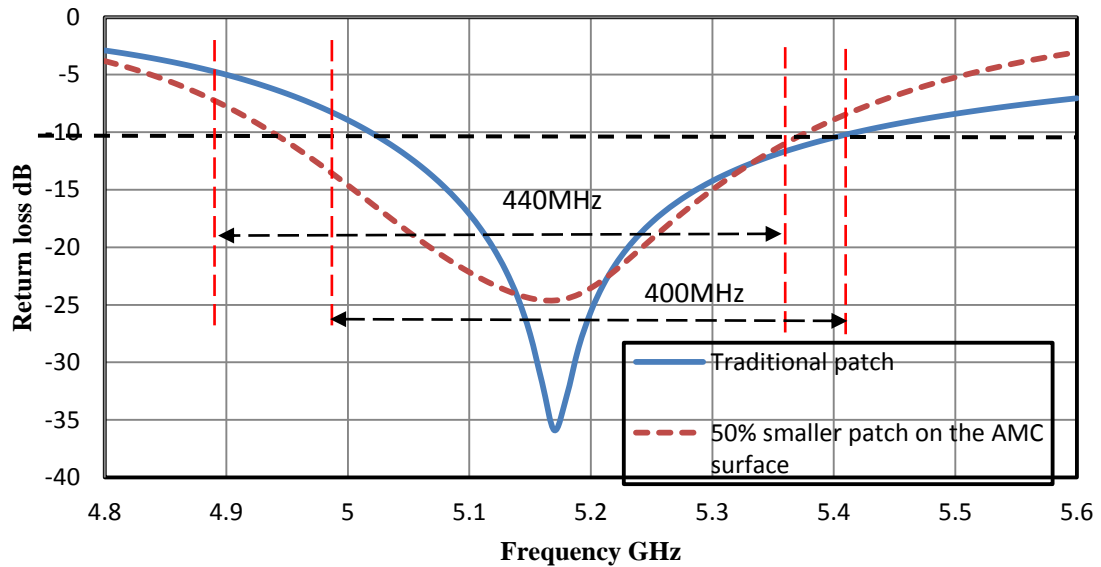


Figure 24: The return loss comparison of the conventional and AMC-based patch antenna

Figure 25 depicts the simulated realized gain performance of the conventional and AMC based patch antennas radiating at 5.17GHz. As seen, the smaller patch has a broadside

gain of 5.16dB which is lower than the 6.95dB gain of the AMC-based patch. The gain drop is due to the smaller antenna size and increased losses associated with the size reduction. The simulated radiation efficiency is 97% for the AMC based patch whereas 99% for conventional patch.

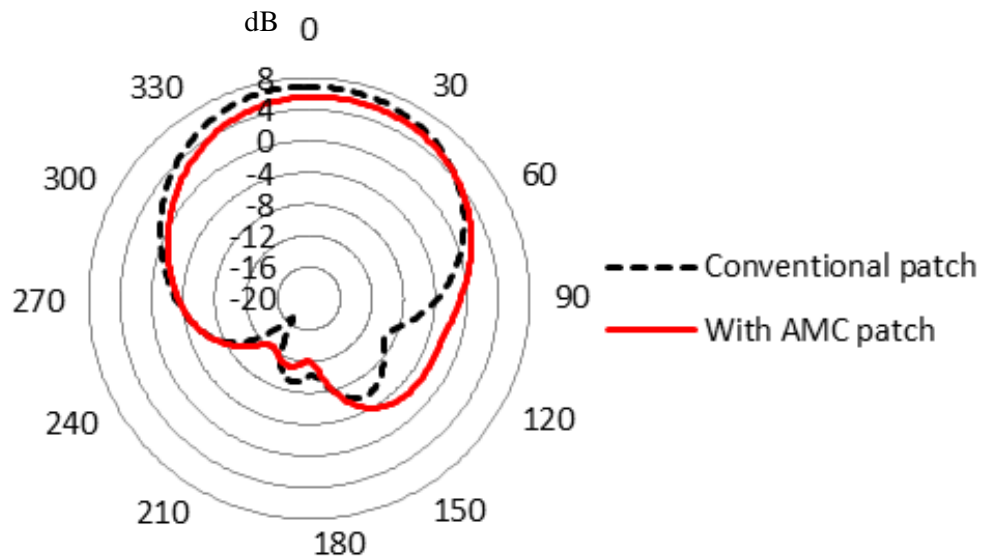
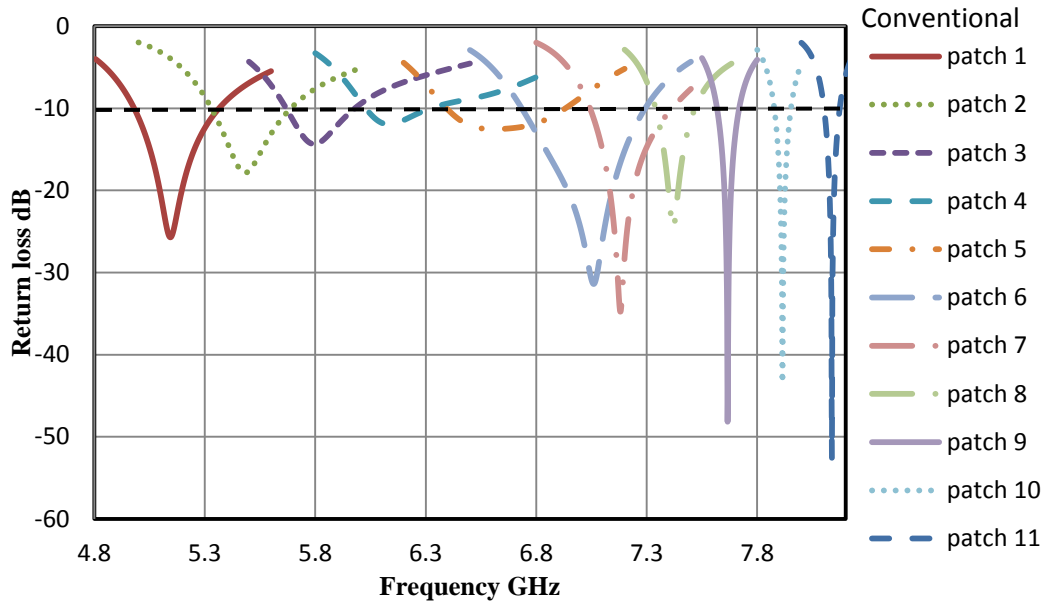
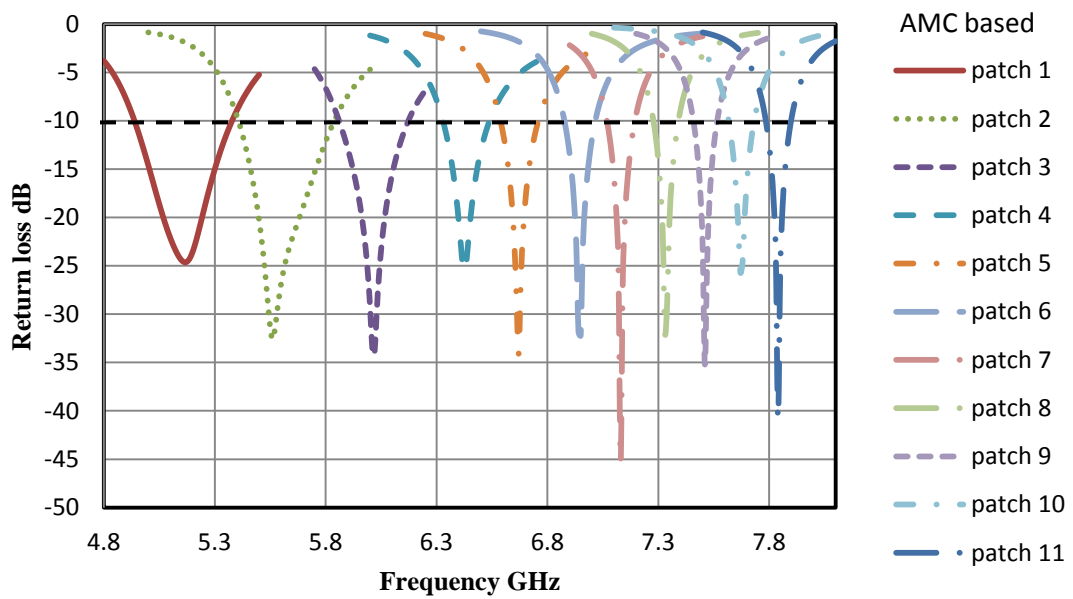


Figure 25: Simulated radiation pattern in $\phi=0$ (y-z plane cut)

The new LPMA design will consist of log-periodic scaled versions of the AMC-based patch antennas. Figure 26 shows the bandwidth performance of 11 conventional antennas that are used in the traditional LPMA design. As seen, the conventional patches making up the traditional LPMA exhibit combined input impedance bandwidth that covers the whole operational (5GHz – 8GHz) band. Likewise, when logarithmically scaled with $\tau=1.07$, 11 AMC based patches also exhibit a collective bandwidth that spans 5GHz -8GHz bandwidth. Hence, the AMC approach is likely to produce a 50% smaller LPMA without scarifying bandwidth and low-profile performance.



(a)



(b)

Figure 26: (a) Simulated return loss performance of the individual patch antennas that makes up the 11 element conventional LPMA, (b) Simulated return loss of 11 log-periodic scaled AMC-based miniature patch antennas.

3.2.4. AMC Design for LPMA

Since each AMC unit cell provides a band limited response, it is not possible to employ a uniform AMC unit cell distribution under a wideband LPMA. Hence, the AMC unit cell must be scaled down in size similar to the scaling preferred in the radiating patch of the LPMA. In our AMC unit cell analysis, we found out that the AMC unit cell can support much larger bandwidth than the patch antenna. Therefore, it may also be possible to utilize a specific AMC unit cell size for a particular group of radiating patches operating at the adjacent resonance frequencies. For example, the AMC unit cell designed in section 3.2.2 displays ~950MHz bandwidth at 5.9GHz whereas the patch that it will be employed for exhibits about 400MHz bandwidth. Hence, it is possible to use the same AMC unit cell size under the two log-periodic scaled patch antennas operating within the vicinity of 5.9GHz.

Based on the above discussion, we investigated two different AMC surface configurations for the LPMA. In the first configuration, each patch antenna within the LPMA centered over an AMC surface has a unit cell layout specifically designed for itself (see Figure 27(a)). In the second configuration, each adjacent three patches are located over single AMC surface that has a -90° to $+90^{\circ}$ reflection bandwidth covering the bandwidth of the whole three patches (see Figure 27(b)).

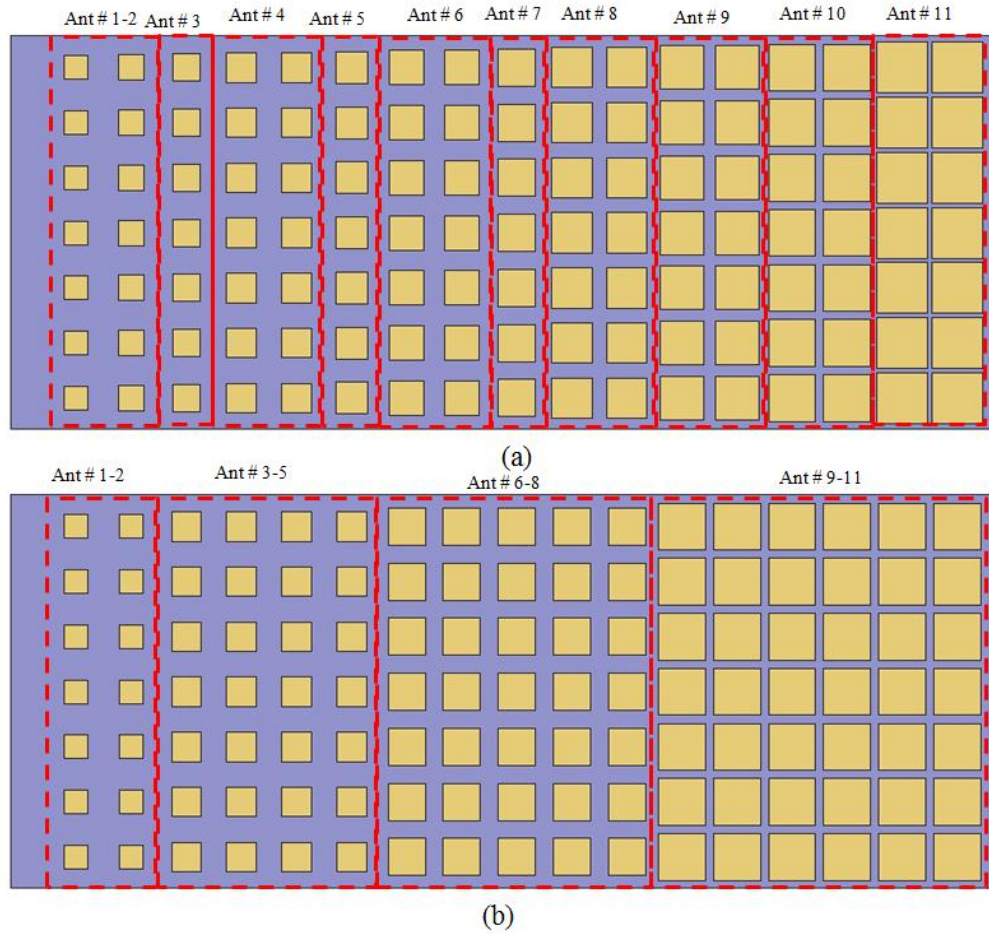


Figure 27: (a) AMC surface configuration #1. (b) AMC surface configuration #2

The scaling of the AMC unit cell groups were performed according to the log-periodic approach. Our numerical simulation demonstrated that the best input impedance mainly is achieved when $\tau=1.08$ is used for the AMC cell groups. It is important note that only the size of the metallic patch within the AMC unit cell was scaled with τ . Hence, as demonstrated in Figure 27, the number of the unit cells along the vertical direction remains the same throughout the structure. This scaling approach was found most attractive one in our numerical simulations for maintaining the wideband impedance of the LPMA. A simulated return loss of surface configuration #2 using same feed line

without the radiating patches of the LPMA is depicted in Figure 28. This result shows that there is not any significant radiation from the AMC unit cells under the open-ended feed line in the 5GHz – 8GHz frequency range.

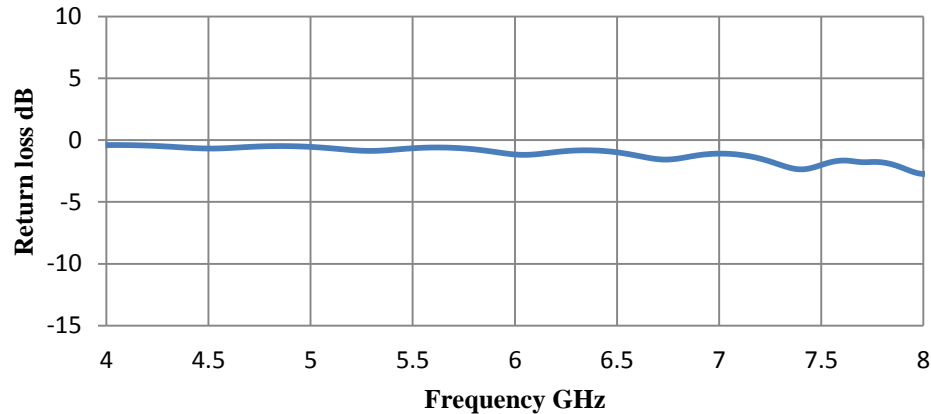


Figure 28: Simulated return loss of surface configuration #2 without radiating patches

3.2.5. Miniature AMC Based LPMA Performance

The LPMA designs over the two AMC surfaces are shown in Figure 29. The simulated return loss and input impedance are provided performance of the antenna in Figure 30 and 31 respectively. These results demonstrate that LPMA with AMC surface configuration #2 perform slightly better than the other AMC based LPMA. Most importantly, the return loss bandwidth is identical to that of the conventional LPMA and covers the whole band of interest (5GHz – 8GHz). To achieve the impedance bandwidth, the overall area between the feed line and the radiating patches has optimized through parametric studies. Also, the middle and bottom substrates were extended by 2.5mm to have a good grip for the SMA connector. Figure 32 shows the current distribution on the AMC-based LPMA with surface configuration #2, to explain the radiation mechanism over the 5GHz – 8GHz band.

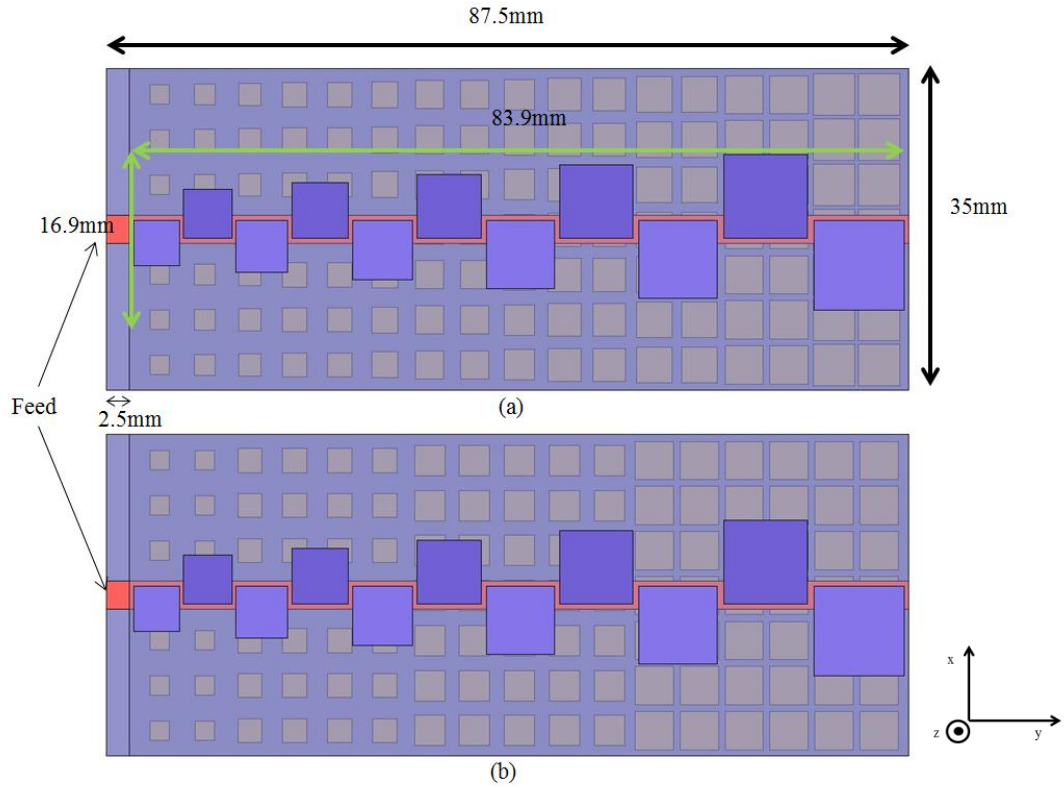


Figure 29: (a) LPMA with AMC surface configuration # 1. (b) LPMA with AMC surface configuration # 2

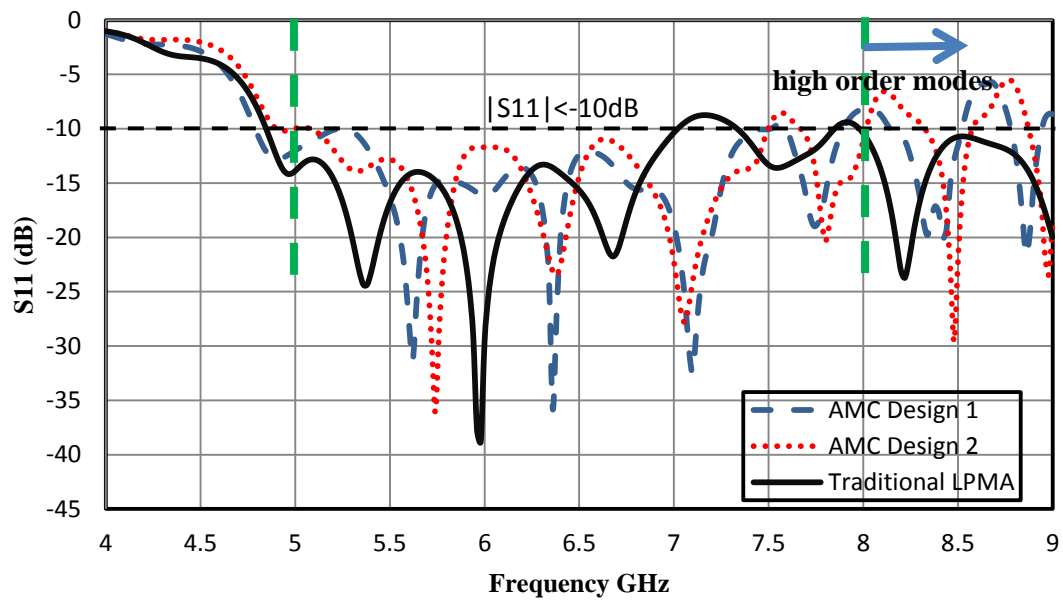


Figure 30: Simulated return loss of the traditional and AMC-based LPMAs

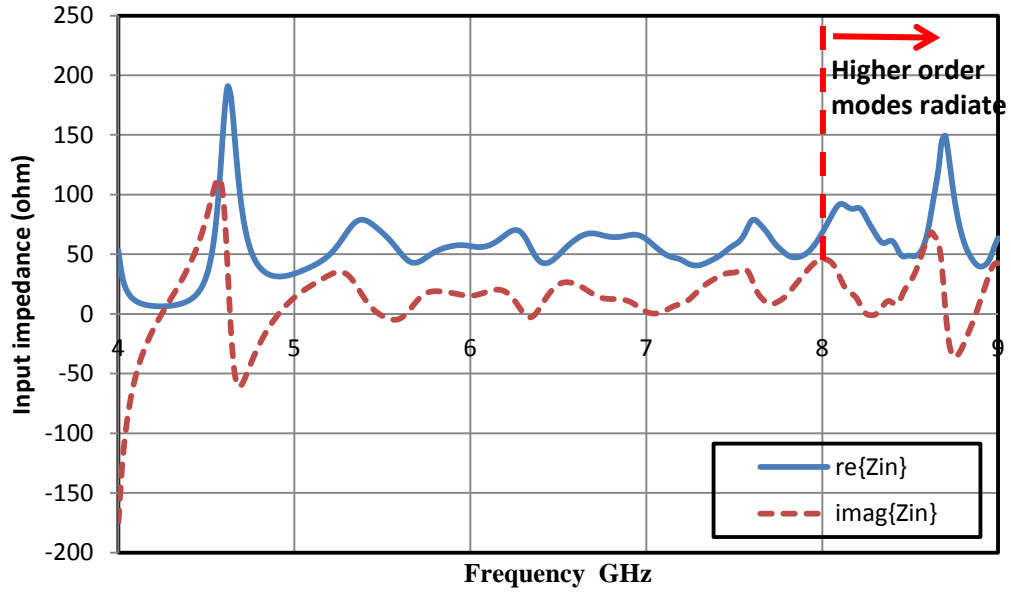
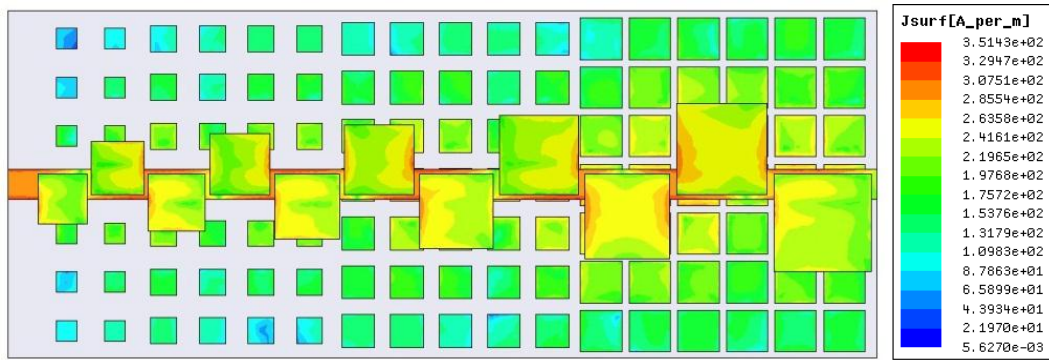
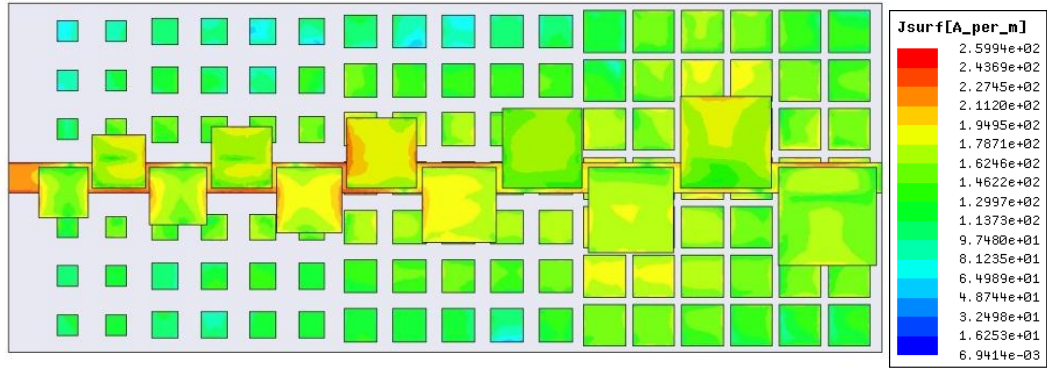


Figure 31: Simulated input impedance of the AMC-based LPMA with surface configuration #1

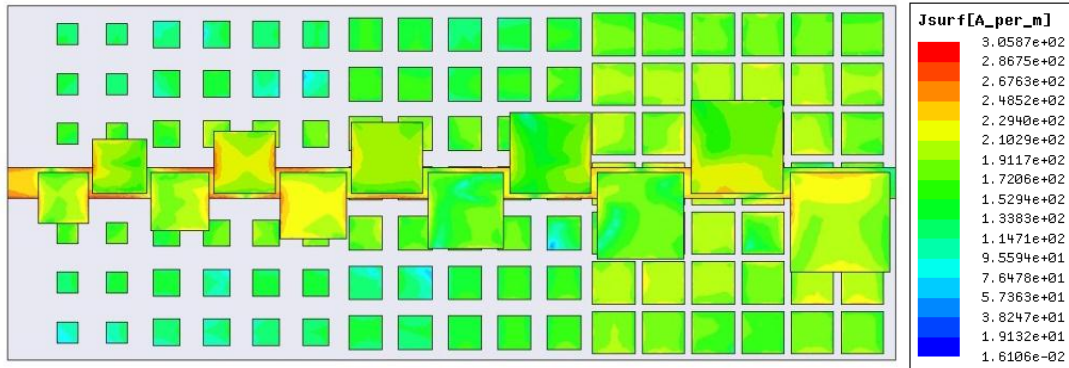


(a)

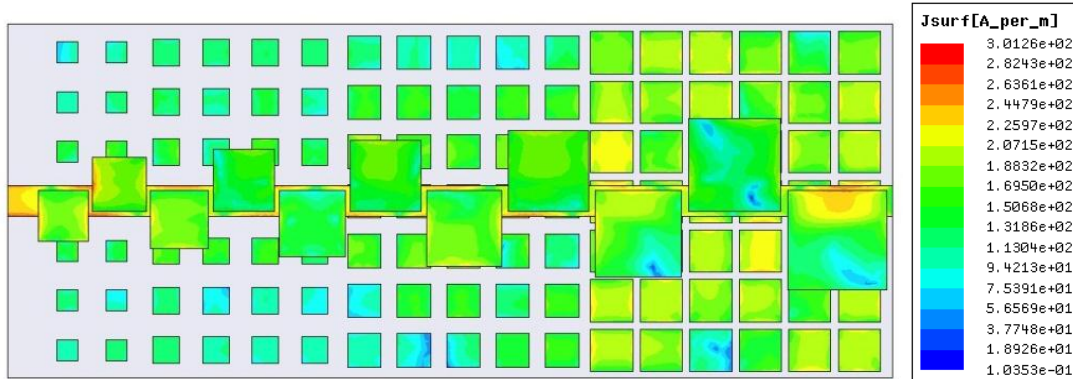
Figure 32: Current distribution on the metallization of AMC-based LPMA with surface configuration #2 (a) 5GHz, (b) 6GHz, (c) 7GHz, (d) 8GHz



(b)



(c)



(d)

Figure 32: (continued)

The simulated realized gain patterns of the LPMA are demonstrated in Figure 33.

Table 1 and 2 provide a summary of the antenna performance in terms of gain and physical size.

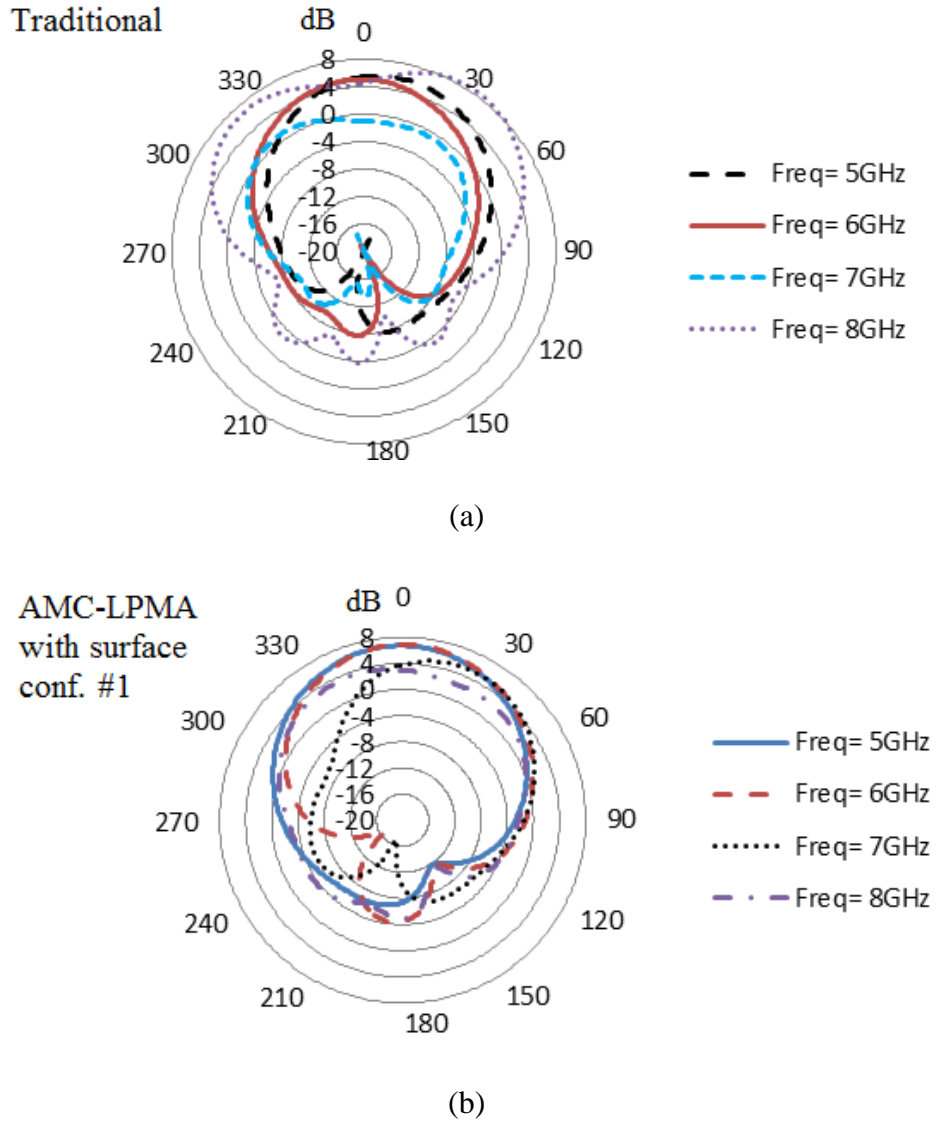
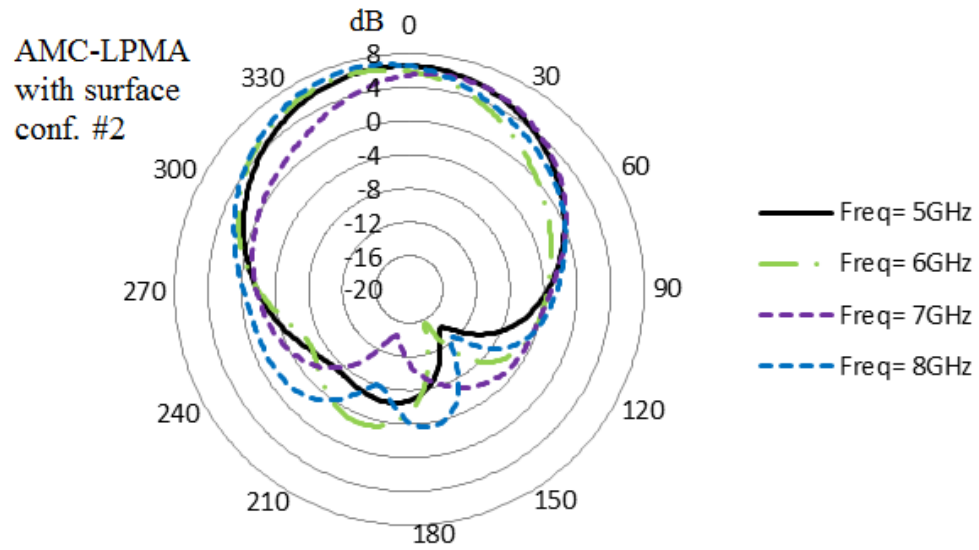


Figure 33: Simulated realized gain in y-z cut for (a) traditional LPMA, (b) with AMC surface configuration #1 (c) with AMC surface configuration #2



(c)

Figure 33: (continued)

Table 1: Size comparison between the traditional and the AMC based LPMA

	Width	Length	Overall Thickness
Traditional	50mm	122.5mm	3.048mm
AMC based	35mm	87.5mm	2.794mm

Table 2: Broadside realized gain comparison between the traditional and AMC-based LPMAs

	Traditional LPMA	AMC-based surface configuration #1	AMC-based surface configuration #2
5GHz	5.45 dB	6.74 dB	6.57 dB
5.5GHz	6.56 dB	5.15 dB	6.89 dB
6GHz	5.11 dB	6.87 dB	5.92 dB
6.5GHz	2.11 dB	3.24 dB	5.62 dB
7GHz	-0.98 dB	3.75 dB	5.44 dB
7.5GHz	4.86 dB	3.04 dB	3.22 dB
8GHz	4.57 dB	3.03 dB	6.59 dB

From the comparisons in table 1 and 2, one can conclude that the AMC-based LPMA provides better gain than the traditional LPMA with surface configuration #2 throughout the 5GHz – 8GHz band. The AMC based LPMA is 50% smaller and has less profile than the conventional antenna. Hence, AMC-based LPMA is more attractive for wideband broadside radiation.

3.2.6. Comments on Design Limitations and Challenges

The 5GHz – 8GHz bandwidth of the LPMA can be further improved by adding more patch radiators. However, this must be done carefully as the proximity feed line has potential to excite higher order modes of the patch antennas. For example, the second mode of the largest patch may exist at the same frequency with the first resonance of a

smaller patch. This can definitely introduce an undesired effect in the impedance matching and must be accounted for using feed line optimization. In addition, the largest AMC unit cells may get coupled from the feeding line which may also radiate undesirably at the same frequency of the small radiating patches.

It is also possible to get more size reduction in the AMC-based LPMA by reducing the total substrate width down to 20mm. However, in this case, the impedance matching gets slightly degraded as can be seen in Figure 34. Specifically, with 20mm substrate size, the LPMA exhibits small frequency ranges within 5GHz – 8GHz band where $|S_{11}| < -10\text{dB}$ is not satisfied. In addition, similar mismatches were observed when the AMC surface configuration shown in Figure 35(a) was applied under the LPMA. As seen, the configuration has a fixed gap size; hence, the overall lateral dimensions of the AMC unit-cell were scaled down (as compared to scaling down the metallic patch of the unit cell).

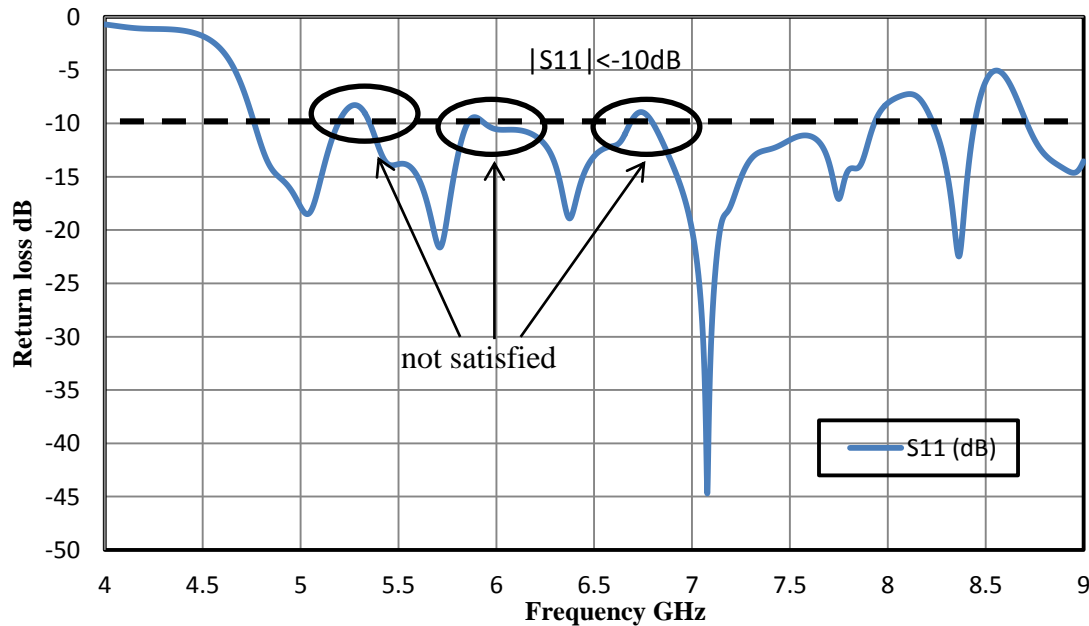
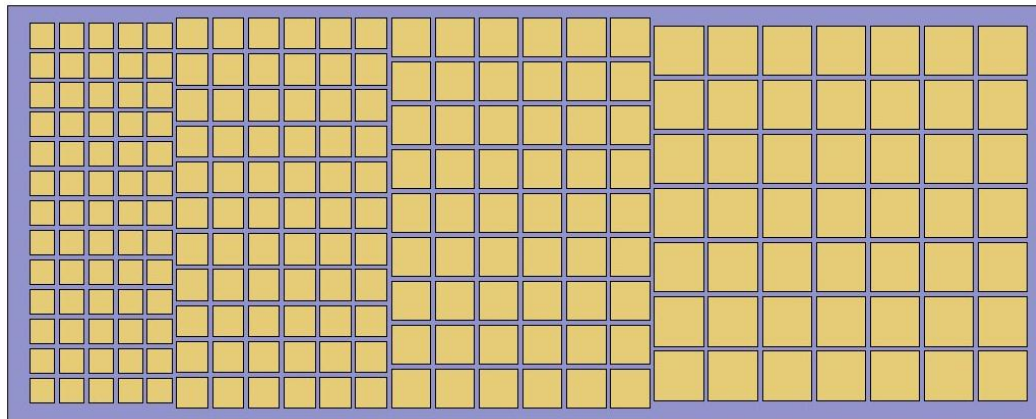
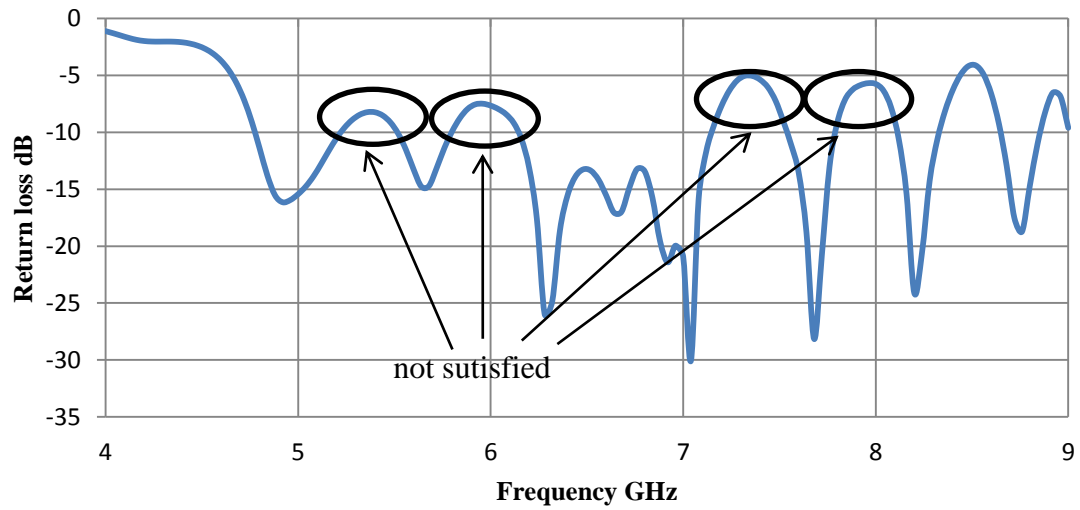


Figure 34: AMC based LPMA configuration #1 with 20mm substrate width



(a)



(b)

Figure 35: (a) AMC based LPMA configuration with fixed 0.4mm spacing metallic patch

(b) Return loss performance of the LPMA on this AMC surface impedance.

3.2.7. Experimental Verification

To verify our simulations, we proceeded with experimental verification. For this, we fabricated the traditional and the AMC-based LPMA (configuration #1 and #2). The antennas were manufactured using two substrate materials: 0.762mm thick Roger RT/duroid 6002 with $\epsilon_r = 2.94$ and 1.27mm thick Roger RT/duroid 6010LM with $\epsilon_r = 10.2$. The traditional LPMA employed four layers of RT/duroid 6002 to realize the 3.048mm overall thickness. The AMC-based LPMA required three layers substrate antennas. The top two are Roger RT/duroid 6002 and the bottom with AMC metallization is Roger RT/duroid 6010LM. Figure 36 shows all the substrate layers of the fabricated antennas. Figure 37 shows the assembled LPMA using nonconductive glue.

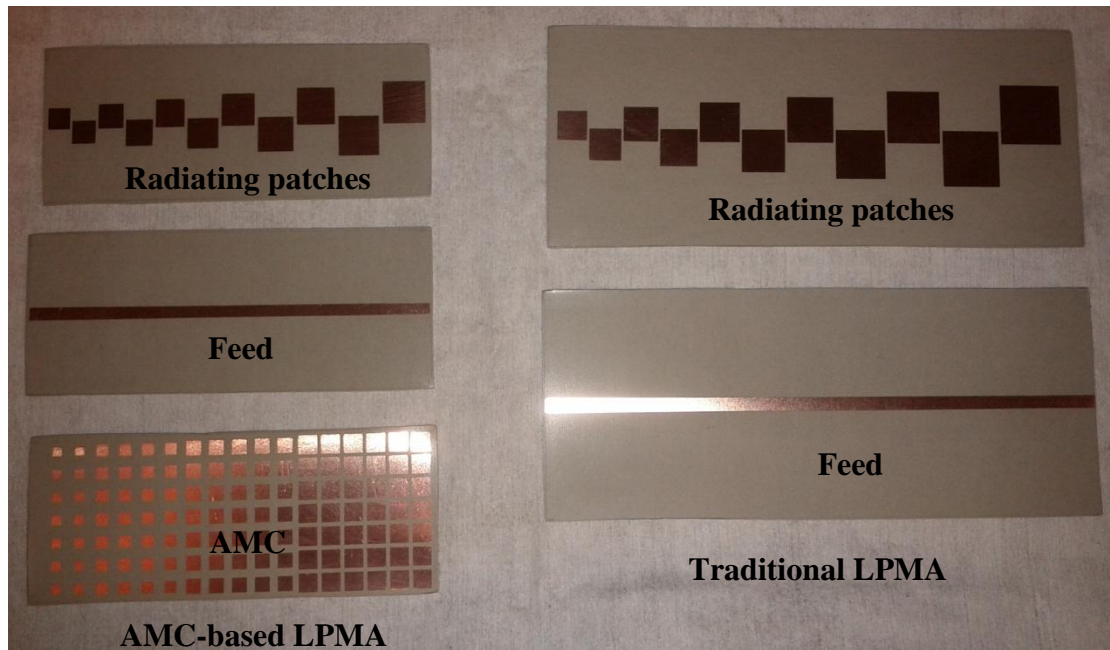


Figure 36: Fabricated substrate layers of the traditional and AMC-based LPMA

Measurements were taken at the anechoic chamber of the University of South Florida Wireless and Microwave Information System (WAMI) laboratory by using a 65GHz Anritsu Lighting vector network analyzer (VNA). Figures 38 through 41 present the simulated and measured return loss performance of the fabricated antennas.

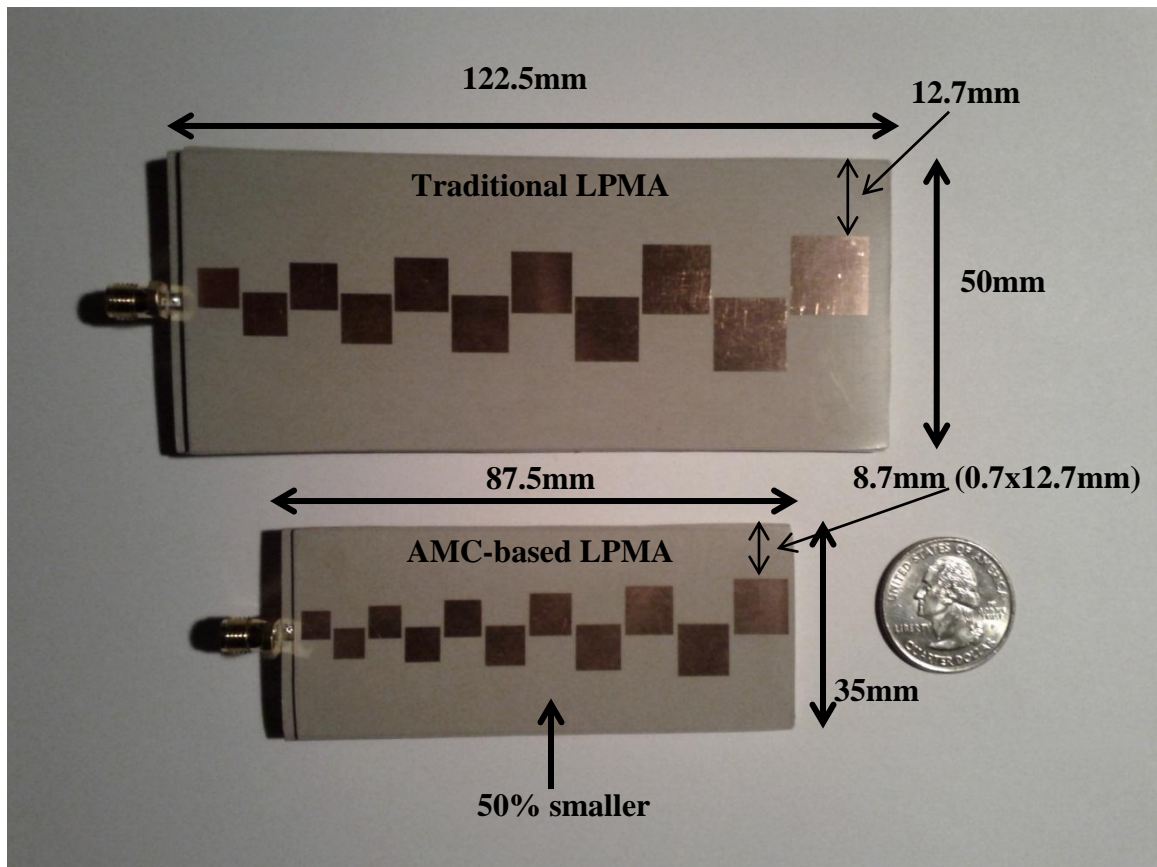


Figure 37: The fabricated LPMA

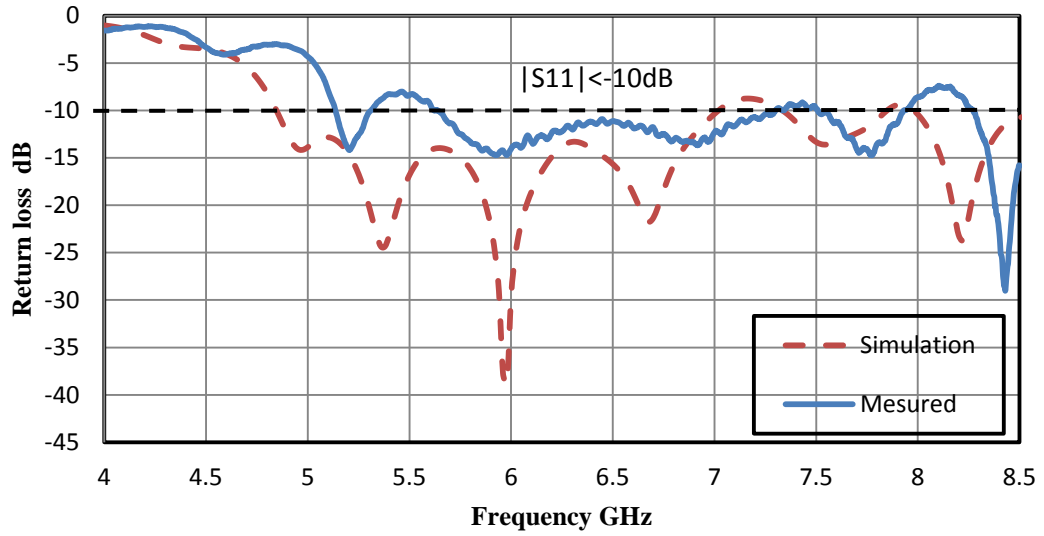


Figure 38: The simulated and measured return loss of the traditional LPMA

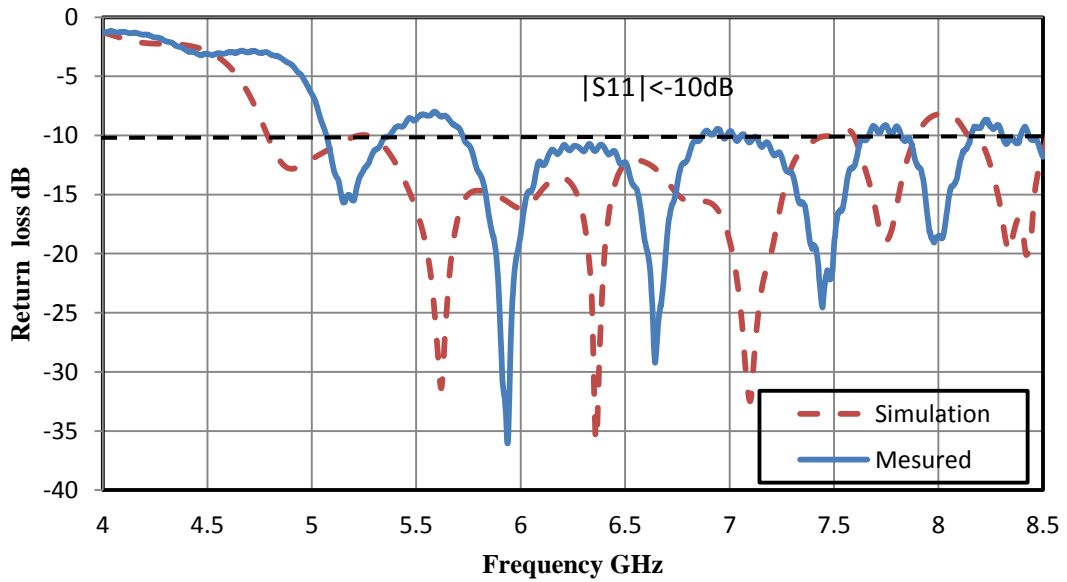


Figure 39: The simulated and measured return loss of the AMC-based LPMA
(configuration #1)

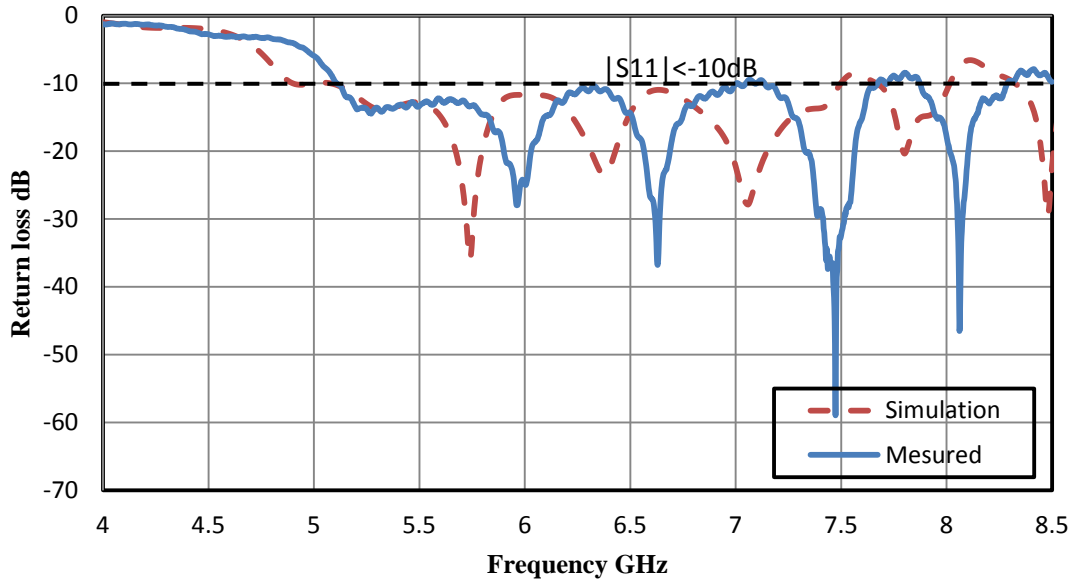


Figure 40: The simulated and measured return loss of the AMC-based LPMA (configuration #2)

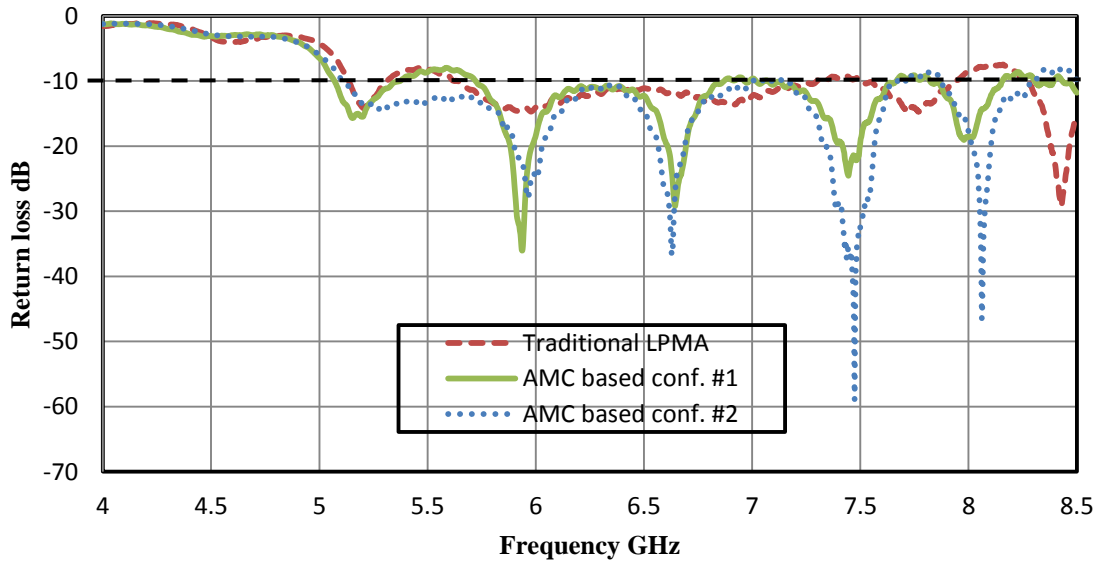
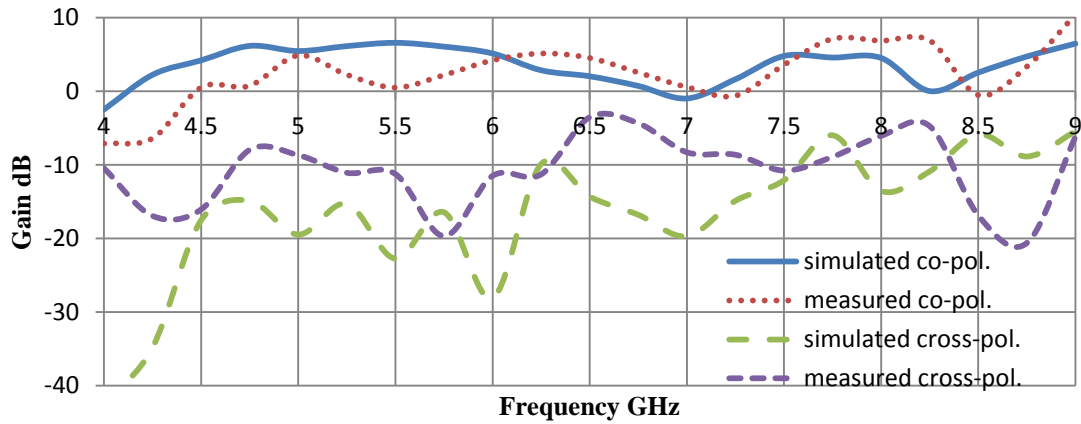
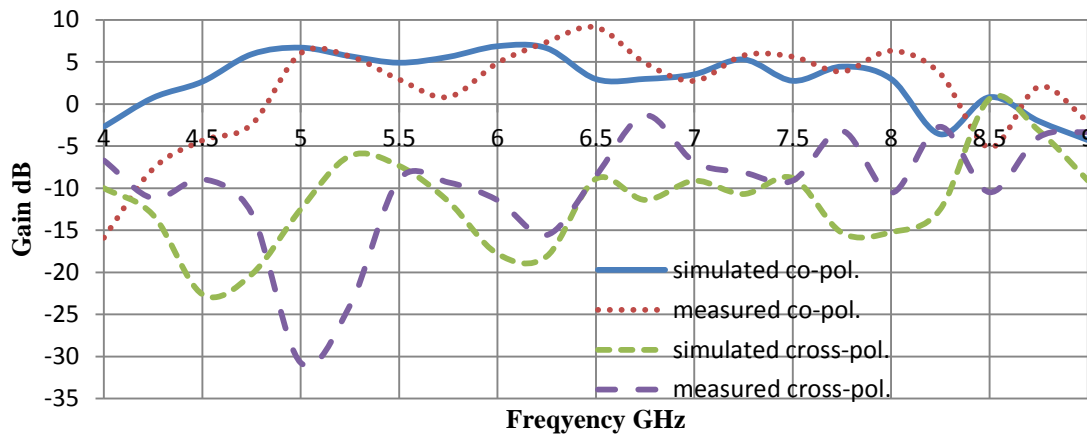


Figure 41: Comparison between the measured return loss of the traditional LPMA and the AMC based LPMA with surface configuration #1 and #2

It is observed that all three fabricated antennas exhibit a similar $\sim 400\text{MHz}$ shift in the lowest frequency where $|S_{11}| < -10\text{dB}$ is achieved (see Figure 41). This can be attributed to the glue layer used to attach the substrates, fabrication errors and inaccuracy in the numerical simulations. Figure 42 (a) – (c) compares the simulated and measured broadside realized co-pol. and cross-pol. gain values. Measure gains patterns in the y-z cut are provided in Figure 43 (a) – (c).

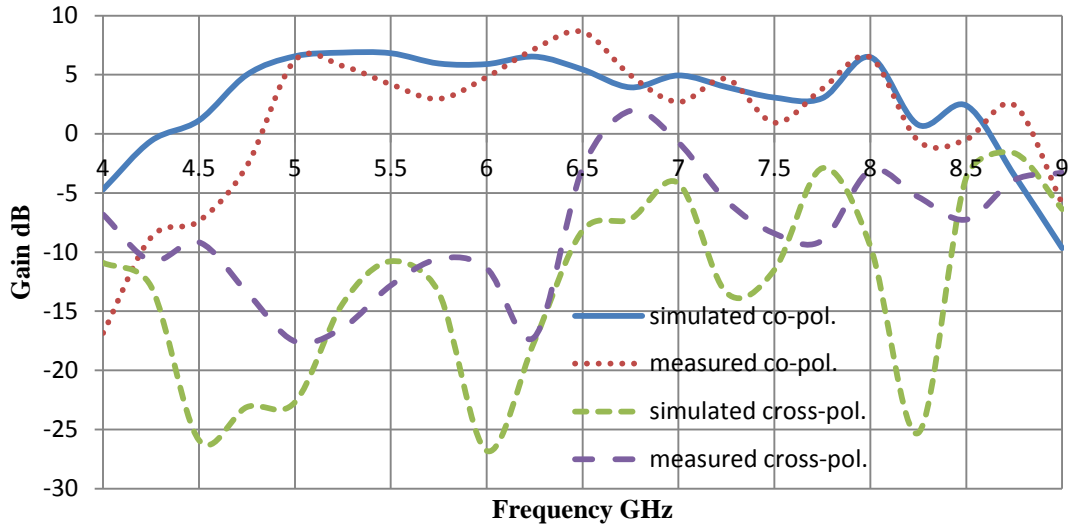


(a)



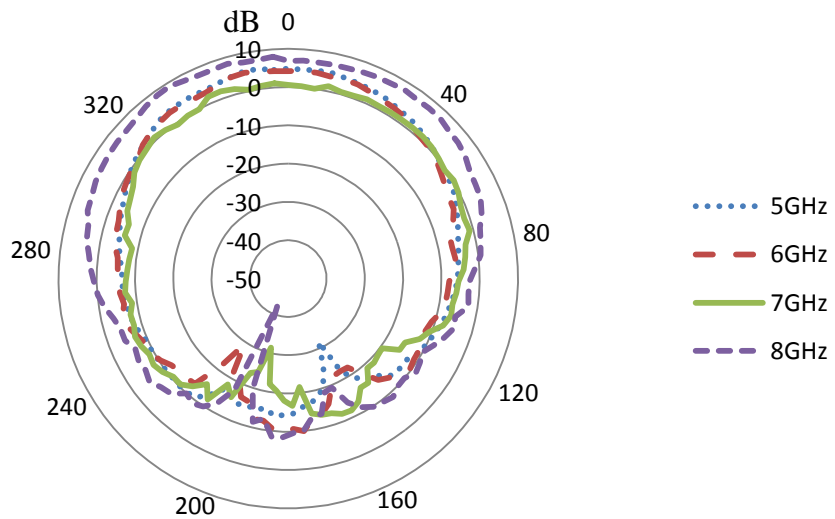
(b)

Figure 42: The simulated and measured broadside gains (a) Traditional LPMA (b) New LPMA with AMC surface 1 (c) New LPMA with AMC surface 2



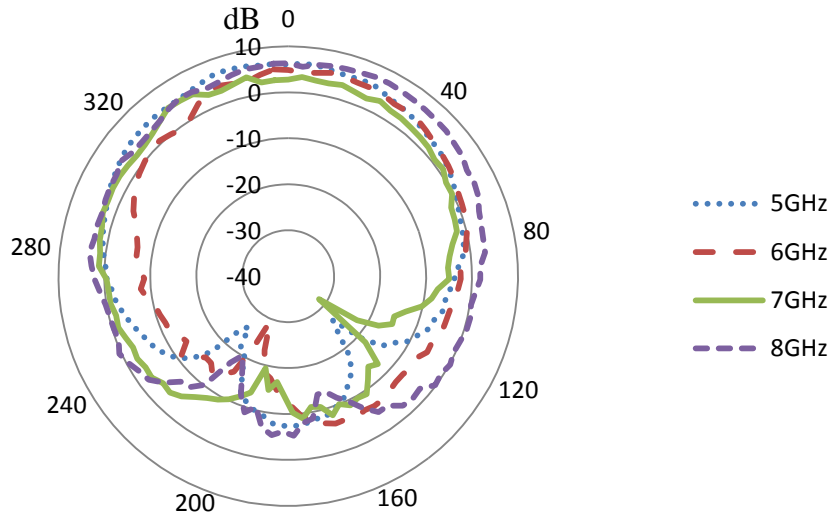
(c)

Figure 42: (continued)

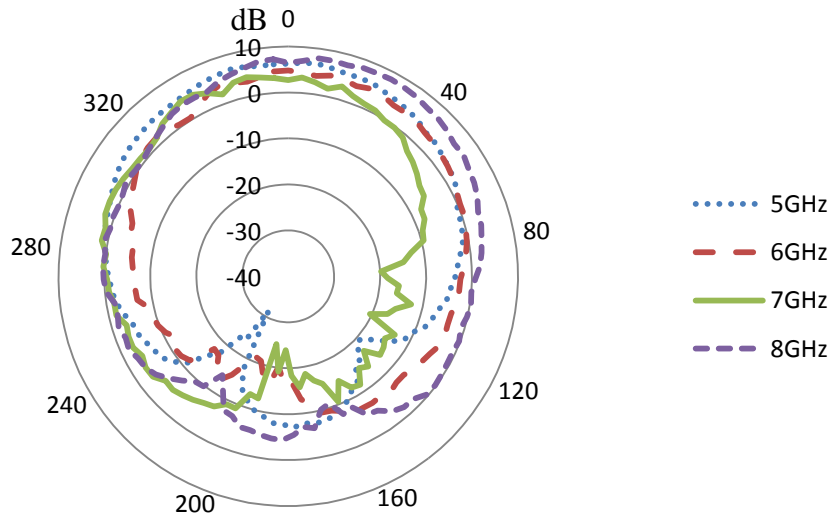


(a)

Figure 43: Measured co-pol. gain pattern in the y-z cut (a) traditional LPMA (b) AMC-based LPMA configuration #1 (c) AMC-based LPMA configuration #2



(b)



(c)

Figure 43: (continued)

From the experimental result, the measured and simulated gain performances of the traditional and AMC-based LPMAs are seen to be in good agreement from 5GHz to 8GHz. The slight differences in broadside radiated gain values can be attributed to the size and position of the SMA connector that was used to feed the LPMAs. Specifically, the employed connector size was large and happened to be near the radiating. From the broadside measured gain pattern, we can observe that the radiation patterns are also somewhat tilted away from the broadside direction in some frequencies. It should be also marked that the patterns were only measured within the y-z plane due to time limitations, but the maximum gain at some frequencies could have been achieved at a different cut. Certainly, more gain measurements need to be taken in different cuts to fully understand this pattern tilting effect. Finally, pattern tilting also occurs due to the close proximity of the adjacent patch elements that could interfere with the radiation of the main radiator.

4. Conclusion

The research motivation for this thesis was miniaturization of LPMA using AMC surfaces. We chose this antenna because of its advantages in terms of low profile, cost, ease of fabrication, light weight and its potential for conformal installations. A proximity coupling technique was used to feed the radiating square patches. Two substrates with different AMC surface realization was introduced and designed to reduce the size of the LPMA.

We demonstrated that the LPMA can be miniaturized by 50%. The design of the AMC surface was carried out to achieve the best return loss in the band from 5GHz – 8GHz. The new antenna has also better gain and radiation pattern in all bands. Because of the low profile and the broadside radiation, this antenna can be mounted on any surface and can be used in radio signal detection and in radar system.

5. Future Work

Different AMC unit cell shapes can be employed and optimized to achieve more size reduction or to enhance the gain performance. Moreover, multiple AMC surfaces with different AMC cell size could be used to miniaturize this antenna. A rectangular patch or slot loaded patch can be used instead of the square ones in order to shift the bandwidth to cover lower frequencies.

References

- [1] de A Filho, V.A.; da F Silva, P.H.; D'Assuncao, A.G.; , "A comparative study of three ultra-wideband log-periodic microstrip antenna arrays," *Antenna Technology (iWAT), 2010 International Workshop on* , vol., no., pp.1-4, 1-3 March 2010
- [2] Sievenpiper, D.; Lijun Zhang; Broas, R.F.J.; Alexopolous, N.G.; Yablonovitch, E.; , "High-impedance electromagnetic surfaces with a forbidden frequency band," *Microwave Theory and Techniques, IEEE Transactions on* , vol.47, no.11, pp.2059-2074, Nov 1999
- [3] Foroozesh, A.; Shafai, L.; , "Investigation Into the Application of Artificial Magnetic Conductors to Bandwidth Broadening, Gain Enhancement and Beam Shaping of Low Profile and Conventional Monopole Antennas," *Antennas and Propagation, IEEE Transactions on* , vol.59, no.1, pp.4-20, Jan. 2011
- [4] Sarabandi, K.; Buerkle, A.M.; Mosallaei, H.; , "Compact Wideband UHF Patch Antenna on a Reactive Impedance Substrate," *Antennas and Wireless Propagation Letters, IEEE* , vol.5, no.1, pp.503-506, Dec. 2006
- [5] Hall, P.S.; , "New wideband microstrip antenna using log-periodic technique," *Electronics Letters* , vol.16, no.4, pp.127-128, February 14 1980
- [6] DuHamel, R.; Isbell, D.; , "Broadband logarithmically periodic antenna structures," *IRE International Convention Record* , vol.5, no., pp. 119- 128, Mar 1957
- [7] Shih-Chang Wu; Alexopoulos, N.G.; , "A log-periodic patch microstrip antenna," *Antennas and Propagation Society International Symposium, 1992. AP-S. 1992 Digest. Held in Conjunction with: URSI Radio Science Meeting and Nuclear EMP Meeting., IEEE* , vol., no., pp.1077-1080 vol.2, 18-25 Jul 1992
- [8] Yang Zhengguang; Su Donglin; Lv Shanwei; , "A novel size-reduced strip line log periodic dipole arrays," *Microwave, Antenna, Propagation and EMC Technologies for Wireless Communications, 2005. MAPE 2005. IEEE International Symposium on* , vol.1, no., pp. 56- 59 Vol. 1, 8-12 Aug. 2005

- [9] Rahim, M.K.A.; Karim, M.N.A.; Masri, T.; Asrokin, A.; "Comparison between Straight and U shape of Ultra Wide Band Microstrip Antenna using Log Periodic Technique," *Ultra-Wideband, 2007. ICUWB 2007. IEEE International Conference on* , vol., no., pp.696-699, 24-26 Sept. 2007
- [10] Gheethan, A.A.; Anagnostou, D.E.; "Reduced size planar Log-Periodic Dipole Arrays (LPDAs) using rectangular meander line elements," *Antennas and Propagation Society International Symposium, 2008. AP-S 2008. IEEE* , vol., no., pp.1-4, 5-11 July 2008
- [11] Strycek, M.; Hertl, I.; "Fractal log-periodic Antenna," *Radioelektronika, 2007. 17th International Conference* , vol., no., pp.1-3, 24-25 April 2007
- [12] Anagnostou, D.E.; Papapolymerou, J.; Tentzeris, M.M.; Christodoulou, C.G.; , "A Printed Log-Periodic Koch-Dipole Array (LPKDA)," *Antennas and Wireless Propagation Letters, IEEE* , vol.7, no., pp.456-460, 2008
- [13] M. N. A Karim, M. K. A. Rahim, H. A. Majid, O. B. Ayop, M. Abu, and F. Zubir, "Log periodic fractal koch antenna for UHF band applications," *Progress In Electromagnetics Research*, Vol. 100, 201-218, 2010
- [14] Mosallaei, H.; Sarabandi, K.; "Novel artificial reactive impedance surface for miniaturized wideband planar antenna design: concept and characterization," *Antennas and Propagation Society International Symposium, 2003. IEEE* , vol.2, no., pp. 403- 406 vol.2, 22-27 June 2003
- [15] Ukkonen, L.; Sydanheimo, L.; Kivikoski, M.; "Patch antenna with EBG ground plane and two-layer substrate for passive RFID of metallic objects," *Antennas and Propagation Society International Symposium, 2004. IEEE* , vol.1, no., pp. 93- 96 Vol.1, 20-25 June 2004
- [16] Jing Liang; Yang, H.Y.D.; , "Analysis of a Proximity Coupled Patch Antenna on a Metalized Substrate," *Antennas and Propagation Society International Symposium 2006, IEEE* , vol., no., pp.2287-2290, 9-14 July 2006
- [17] Qu, D.; Shafai, L.; Foroozesh, A.; , "Improving microstrip patch antenna performance using EBG substrates," *Microwaves, Antennas and Propagation, IEE Proceedings -* , vol.153, no.6, pp.558-563, Dec. 2006
- [18] Al-Nuaimi, M.K.T.; Whittow, W.G.; "Novel planar AMC for low profile antenna applications," *Antennas & Propagation Conference, 2009. LAPC 2009. Loughborough* , vol., no., pp.145-148, 16-17 Nov. 2009
- [19] Al-Nuaimi, M.; , "Low profile dipole antenna design using square SRRs artificial ground plane," *Wireless Conference (EW), 2010 European* , vol., no., pp.190-193, 12-15 April 2010

- [20] de Cos, M.E.; Alvarez, Yu.; Hadarig, R.C.; Las-Heras, F.; , "Novel SHF-Band Uniplanar Artificial Magnetic Conductor," *Antennas and Wireless Propagation Letters, IEEE* , vol.9, no., pp.44-47, 2010
- [21] Sohn, J. R., K. Y. Kim, and H.-S. Tae, "Comparative study on various artificial magnetic conductors for low-profile antenna," *Progress In Electromagnetics Research, PIER* 61, 27{37, 2006.
- [22] Kovács, P.; Raida, Z.; Lukeš, Z.; , "Design and optimization of periodic structures for simultaneous EBG and AMC operation," *Microwave Techniques (COMITE), 2010 15th International Conference on* , vol., no., pp.195-198, 19-21 April 2010
- [23] Calhau, Luis; Pinho, Pedro; , "Low profile multi-band antenna for mobile communications," *Antennas and Propagation (EuCAP), 2010 Proceedings of the Fourth European Conference on* , vol., no., pp.1-4, 12-16 April 2010
- [24] Grange, F.; Delaveaud, C.; Madhjoubi, K.; , "Miniaturization of artificial magnetic conductors," *Antennas and Propagation Society International Symposium (APSURSI), 2010 IEEE* , vol., no., pp.1-4, 11-17 July 2010
- [25] Ranga, Y.; Matekovits, L.; Esselle, K.P.; Weily, A.R.; , "Multioctave Frequency Selective Surface Reflector for Ultrawideband Antennas," *Antennas and Wireless Propagation Letters, IEEE* , vol.10, no., pp.219-222, 2011
- [26] Al-Nuaimi, Mustafa K. Taher; Whittow, William G.; , "Low profile dipole antenna backed by isotropic Artificial Magnetic Conductor reflector," *Antennas and Propagation (EuCAP), 2010 Proceedings of the Fourth European Conference on* , vol., no., pp.1-5, 12-16 April 2010
- [27] Salonen, P.; Keskilammi, M.; Rahmat-Samii, Y.; , "Textile antennas: Effect of antenna bending on radiation pattern and efficiency," *Antennas and Propagation Society International Symposium, 2008. AP-S 2008. IEEE* , vol., no., pp.1-4, 5-11 July 2008
- [28] de Cos, M.E.; Las Heras, F.; Franco, M.; , "Design of Planar Artificial Magnetic Conductor Ground Plane Using Frequency-Selective Surfaces for Frequencies Below 1 GHz," *Antennas and Wireless Propagation Letters, IEEE* , vol.8, no., pp.951-954, 2009
- [29] Yang Wenwen; Hua Guang; Hong Wei; , "Wideband artificial magnetic conductor structure for Ku-band antenna applications," *Microwave, Antenna, Propagation and EMC Technologies for Wireless Communications, 2009 3rd IEEE International Symposium on* , vol., no., pp.954-957, 27-29 Oct. 2009

- [30] Duan, Z.; Linton, D.; Scanlon, W.; Conway, G.; , "Using EBG to Improve Antenna Efficiency in Proximity to the Human Body," *Wideband, Multiband Antennas and Arrays for Defence or Civil Applications, 2008 Institution of Engineering and Technology Seminar on* , vol., no., pp.173-180, 13-13 March 2008
- [31] Niyomjan, G.; Huang, Y.;, "A suspended microstrip fed slot antenna on high impedance surface structure," *Antennas and Propagation, 2006. EuCAP 2006. First European Conference on* , vol., no., pp.1-4, 6-10 Nov. 2006
- [32] Costa, F.; Genovesi, S.; Monorchio, A.;, "On the bandwidth of printed frequency selective surfaces for designing high impedance surfaces," *Antennas and Propagation Society International Symposium, 2009. APSURSI '09. IEEE* , vol., no., pp.1-4, 1-5 June 2009
- [33] Balanis, C.A., *Antenna Theory: Analysis and Design*, John Wiley & Sons, Inc, 2005.
- [34] Hall, P.S.; , "Bandwidth limitations of log-periodic microstrip patch antenna arrays," *Electronics Letters* , vol.20, no.11, pp.437-438, May 24 1984
- [35] Isbell, D.; , "Log periodic dipole arrays," *Antennas and Propagation, IRE Transactions on* , vol.8, no.3, pp.260-267, May 1960
- [36] Hall, P.S.; , "Multioctave bandwidth log-periodic microstrip antenna array," *Microwaves, Antennas and Propagation, IEE Proceedings H* , vol.133, no.2, pp.127-136, April 1986
- [37] Smith, H.K.; Mayes, P.E.; , "Log-periodic array of dual-feed microstrip patch antennas," *Antennas and Propagation, IEEE Transactions on* , vol.39, no.12, pp.1659-1664, Dec 1991
- [38] Romodin, V.B.; Oznobikhin, V.I.; Kopylov, V.V.;, "Log periodic microstrip array," *High Power Microwave Electronics: Measurements, Identification, Applications, 1999. MIA-ME '99. Proceedings of the IEEE-Russia Conference* , vol., no., pp.IV4-IV6, 1999
- [39] Campbell, C.; Traboulay, I.; Suthers, M.; Kneve, H.; , "Design of a stripline log-periodic dipole antenna," *Antennas and Propagation, IEEE Transactions on* , vol.25, no.5, pp. 718- 721, Sep 1977
- [40] Scheuring, A.; Wuensch, S.; Siegel, M.; , "A Novel Analytical Model of Resonance Effects of Log-Periodic Planar Antennas," *Antennas and Propagation, IEEE Transactions on* , vol.57, no.11, pp.3482-3488, Nov. 2009

- [41] Qi Wu; Ronghong Jin; Junping Geng; , "A Single-Layer Ultrawideband Microstrip Antenna," *Antennas and Propagation, IEEE Transactions on* , vol.58, no.1, pp.211-214, Jan. 2010
- [42] Yang, F. and Y. Rahmat-Samii, *Electromagnetic Band Gap Structures in Antenna Engineering*, Cambridge University Press, 2009.
- [43] Ying-Ying Gu; Wen-Xun Zhang; Zhi-Chen Ge; Zhen-Guo Liu; , "Research on reflection phase characterizations of artificial magnetic conductors," *Microwave Conference Proceedings, 2005. APMC 2005. Asia-Pacific Conference Proceedings* , vol.3, no., pp. 4 pp., 4-7 Dec. 2005
- [44] Yousefi, L.; Mohajer-Iravani, B.; Ramahi, O.M.; , "Enhanced Bandwidth Artificial Magnetic Ground Plane for Low-Profile Antennas," *Antennas and Wireless Propagation Letters, IEEE* , vol.6, no., pp.289-292, 2007
- [45] Bao, X.L.; Ammann, M.J.;, "Design of Compact Multi-band EBG Structures," *Antennas and Propagation, 2007. EuCAP 2007. The Second European Conference on* , vol., no., pp.1-4, 11-16 Nov. 2007
- [46] Foroozesh, A.; Shafai, L.; , "Application of combined electric- and magnetic-conductor ground planes for antenna performance enhancement," *Electrical and Computer Engineering, Canadian Journal of* , vol.33, no.2, pp.87-98, Spring 2008
- [47] Vu Van Yem; Tran The Phuong; , "Ultra-wide band low-profile spiral antennas using an EBG ground plane," *Advanced Technologies for Communications (ATC), 2010 International Conference on* , vol., no., pp.89-94, 20-22 Oct. 2010
- [48] Horii, Y.; Tsutsumi, M.;, "Wide band operation of a harmonically controlled EBG microstrip patch antenna," *Antennas and Propagation Society International Symposium, 2002. IEEE* , vol.3, no., pp. 768- 771, 2002
- [49] Ying Zhang; von Hagen, J.; Younis, M.; Fischer, C.; Wiesbeck, W.; , "Planar artificial magnetic conductors and patch antennas," *Antennas and Propagation, IEEE Transactions on* , vol.51, no.10, pp. 2704- 2712, Oct. 2003
- [50] McKinzie, W.; Rogers, S.;, "A multi-band artificial magnetic conductor comprised of multiple FSS layers," *Antennas and Propagation Society International Symposium, 2003. IEEE* , vol.2, no., pp. 423- 426 vol.2, 22-27 June 2003
- [51] Kern, D.J.; Werner, D.H.; Werner, P.L.;, "Optimization of multi-band AMC surfaces with magnetic loading," *Antennas and Propagation Society International Symposium, 2004. IEEE* , vol.1, no., pp. 823- 826 Vol.1, 20-25 June 2004

- [52] Jing Liang; Yang, H.Y.D.; , "Microstrip Patch Antennas on Tunable Electromagnetic Band-Gap Substrates," *Antennas and Propagation, IEEE Transactions on* , vol.57, no.6, pp.1612-1617, June 2009
- [53] Qi Luo; Pereira, J.R.; Salgado, H.M.; , "Tunable multiband antenna with an active artificial magnetic conductor ground plane," *Microwave Conference (EuMC), 2010 European* , vol., no., pp.461-464, 28-30 Sept. 2010